NTNU – Trondheim
Norwegian University of
Science and Technology

Emotion Recognition in EEG

A neuroevolutionary approach

Stian Pedersen Kvaale

Master of Science in Computer Science
Submission date: June 2012
Supervisor: Asbjørn Thomassen, IDI

Norwegian University of Science and Technology
Department of Computer and Information Science

Problem Description

Study how to recognize emotions defined by an accepted psychological model, in EEG, by the use of an artificial neural network. This entails an investigation of the problem areas (Emotions, EEG, and Brain Computer Interfaces), commonly used computational methods in these areas, and an overview of systems previously described in the literature with similar goals. This should result in a method and an implementation that accomplish the goal of recognizing different emotions in EEG.

Assignment given: January 16th, 2012
Supervisor: Asbjørn Bløtekjær Thomassen

Abstract

Ever since the invention of EEG have constant attempts been made to give meaning to the oscillating signal recorded. This has resulted in the ability to detect a wide range of different psychological and physiological phenomenon. The goal of this thesis is to be able to recognize different emotions in EEG by the use of a computer and artificial intelligence.

Emotions are an especially interesting phenomenon because of the huge impact they have on humans on the daily basis. They constantly guides and modulates our rationality, and is thus in some sense an important part of the definition of human rationality, which again plays an important role in how we behave intelligently and especially how we behave intelligently when interacting with other humans.

Machines that interact with humans do however not base their decisions on a rationality that incorporates live human emotions. The effect of this mismatch in rationality between humans and machines results in unwanted behaviour from the machines, and is something most have experienced. The system we propose in this thesis could be used to allow machines to incorporate an interpretation of human emotions in their principles of rationality, in the form of a recognized two-dimensional model of emotions, which could result in a more intelligent interaction with humans. We further restricted our system to the hardware limitations of the commercially available Emotiv EPOC EEG headset, in order to get an indication of the commercial value and general implications of our method.

Both unsuccessful and successful systems with similar goals have previously been described in the literature. These systems typically rely on computationally expensive feature extractions, which make them less attractive when a relatively quick response is needed. Moreover, the act of choosing what methods to use in order to extract features entails a degree of subjectivity from the creator, which becomes clear by looking at the share variety of completely different methods used in the different systems.

Our system effectively minimizes both of these issues by presenting the signal as it is, expressed in the frequency domain, to an artificial neural network trained by a neuroevolutionary method called HyperNEAT, with promising results. This highlights the importance of using a method that is truly in line with nature of the problem.

Sammendrag

Helt siden oppfinnelsen av EEG har det kontinuerlig blitt gjort forsøk på å tolke signalet man har registrert. Resultatet av dette har gitt oss mulighet til å oppdage et bredt spekter av ulike psykologiske og fysiologiske fenomen via EEG. Målet i denne oppgaven er å gjenkjenne forskjellige følelser i EEG, ved bruk av en datamaskin og kunstig intelligens.

Følelser er et spesielt interessant fenomen på grunn av den store påvirkningen de har på oss mennesker. Siden vår rasjonalitet kontinuerlig blir guidet og modulert av følelser, er de dermed til en viktig del av definisjonen av menneskelig rasjonalitet. Dette spiller igjen en viktig rolle i hvordan vi oppfører oss intelligent, og spesielt hvordan vi oppfører oss intelligent når vi er i interaksjon med andre mennesker.

Maskiner som er i interaksjon med mennesker baserer i midlertidig ikke sine beslutninger på en rasjonalitet som inkluderer menneskelige følelser. Disse forskjellene i rasjonalitetsprinsipper mellom mennesker og maskiner kan enkelt sees gjennom uønsket atferd fra maskiner, noe som de fleste har opplevd. Systemet vi foreslår i denne avhandlingen kan brukes til å tillate maskiner å innlemme en tolkning av menneskelige følelser i sine prinsipper om rasjonalitet, i form av en anerkjent todimensjonal modell av følelser, noe som kan resultere i en mer intelligent interaksjon med mennesker. For å få en indikasjon på den kommersielle verdien og de generelle implikasjonene av vår metode, har vi begrenset vårt system til å kunne støtte det kommersielt tilgjengelige Emotiv EPOC EEG-apparatet.

Både mislykkede og vellykkede systemer med lignende mål har tidligere blitt beskrevet i litteraturen. De fleste av disse er avhengige av mål og beskrivelser av signalet som er kostbare beregningsmessig, noe som gjør dem mindre attraktive når en trenger relativt rask responstid. Dette innebærer også en viss subjektivitet fra skaperen av systemet når man skal velge hvilke mål og beskrivelser man skal bruke, noe som kommer tydelig frem ved å se på alle de ulike metodene som brukes i de ulike systemene.

Vårt system minimerer effekten av begge disse problemene ved å presentere signalet som det er, uttrykt i frekvenser, til et kunstig nevralt nettverk som er trent av en nevroevolusjonær metode som kalles HyperNEAT, med lovende resultater. Dette understreker viktigheten av å bruke en metode som virkelig er i tråd med problemets natur.

Preface

This master thesis is a continuation of my specialization project conducted in the autumn 2012, and is a part of my degree in Computer Science, with a specialization in Intelligent Systems, at the Department of Computer and Information Science (IDI), in the Faculty of Information Technology, Mathematics and Electrical Engineering (IME), at the Norwegian University of Science and Technology (NTNU).

My motivations for writing this thesis are my general interest in psychology (including most sub-disciplines), computational models of mental phenomena, and their link to bio-inspired artificial intelligence methods, as well as sub-symbolic artificial intelligence in general. I am also intrigued by intelligent user interfaces, and what the field of affective computing can contribute to this field, when dealing with people in real-life situations.

I would especially like to thank my supervisor, assistant professor Asbjørn Bløtekjær Thomassen for the valuable guidance and feedback throughout this process, and for supporting me in taking a multi-disciplinary approach to the challenges entailed by the problems investigated in this thesis. I would also like to thank my dear family, friends, and fellow AI students, for the supportive, inspirational, and constructive feedback throughout this process period.

Trondheim, June 11th, 2012
Stian P. Kvaale

Contents

Let's not forget that the little emotions are the great captains of our lives, and that we obey them without realizing it.

— *Vincent Van Gogh (1889)*

Chapter 1

Introduction

As early as in 1924 did Hans Berger, a German neurologist, record the first electroencephalogram (EEG) from a human being. An EEG shows the synchronized neuronal activity from a region of a brain, recorded by an electrode as an oscillating signal reflecting the electric potential from the group of neurons situated in close proximity to the electrode. This recording was in the early days only suitable for detecting large differences seen in the pattern produced, such as epileptic seizures, because the quality of the recording instrument and the fact that one had to manually inspect the waveform produced in order to identify changes in the rhythms of the brain. Along with more precise recording equipment, empirical studies of EEG, and the availability of sufficient computational power in modern computers, came the rise of the ability to detect even more subtle changes in the electric potential recorded. These subtle changes have been recognized to encode for cognitive processes such as selective attention, working memory, mental calculations, as well as specific cognitive states and different types of behaviour (Nunez and Srinivasan, 2006, 2007).

Motivated by the detection of progressively more subtle and intricate changes in EEG that encodes for even more subtle and intricate mental phenomena, we start our ambitious quest of detecting human emotions in EEG. There are many mental phenomena that we find interesting, but emotions stand out from all of these as the most interesting and important to us because of the huge impact they have on the daily basis of humans. Emotions constantly guides and modulates our rationality, and is thus in some sense an important part of the definition of human rationality, which again plays an important role in how we behave intelligently and especially how we behave intelligently when interacting with other humans.

This implies that emotions probably must be incorporated in machines in order

to achieve strong artificial intelligence (human like intelligence). While the thought of giving machines the ability to base their decisions and behaviour on a rationality that includes their own register of emotions is compelling, we find it even more important that they base their decisions and behaviour on a rationality that incorporates human emotions when they are directly or indirectly interacting with humans through an interface.

We believe that most have seen how wrong things can go because of the rationality mismatch between machines and humans, but let us illustrate it with a typical scenario. John Smith buys a new computer with the most common operating system (OS) pre-installed. Eager to get started with his new technological investment, he quickly accepts the recommendation from the machine that all future updates of the OS should be handled automatically in the background by the system itself. Then one day when he gets back from lunch, he discovers that the machine has rebooted by itself. Unfortunately, John Smith does only make backups every afternoon before going home from work, so half a day worth of work is lost along with his train of thought. When he logs in on his account on the machine, a festive (but totally inappropriate) note appears in the lower right corner of the screen stating: "Congratulations! The OS has successfully been updated, and you are now safe from outside threats."

The machine found it rational to reboot even though John Smith was in the middle some important work, and that losing this work would clearly upset him. An ideal scenario would be that the machine assessed how upset John Smith would be if he lost the unsaved work, compared to how upset he would be because of the consequences of not updating the system immediately. A sub-optimal behaviour could be that the machine actually made the reboot, but learnt from John's frustration after losing his work, and modulated its behaviour to never again reboot without permission.

So by allowing the machine to incorporate an interpretation of human emotions, a more mutual understanding of what is rational could be achieved, which again could result in less unwanted behaviour from the machine when interacting with humans.

We have, up until now, used the word emotions quite recklessly under the assumption that there is a universal consensus in how to describe different emotions. This is not the case; emotions are indeed a subjective experience, and the ability to communicate any emotion felt is limited by a person's psychological and physiological abilities, as well as prior experiences and the language used. The word happy

is often used to describe an emotion, and most would agree that there is an approximately universal consensus about the meaning of this particular word. However, when dealing with self-reported data on emotions, it turns out that there is a great variation in the data collected because of the different interpretations of descriptions of emotions, which leads to uncertainty in the results from any analysis of this data. This has led to research on universal models of emotions, which accounts for most of the variance introduced by self-assessments of emotions.

We rely on one of these models in this thesis in order to get reliable answers when testing our method of automatically detecting emotions through EEG. By doing so, we allow the system to generalize over the (more or less) universal cognitive interpretation of emotions, instead of a system that generalizes over pure subjectivity. We believe that this is an important aspect, because comparing the results from different subjects in a system that is not based on a statistically sound model of emotions would lead to answers that comes with an uncertainty that is not accounted for.

This thesis does also explore brain-computer interfaces (BCI) in order to find commonly used computational methods for interpretation and analysis of data that stems from brain activity, and to recognize what different types of systems that exist. The most interesting parts of this exploration are of course the systems that use EEG and artificial neural networks, as it is the main focus given our problem description. To add further constrains, should the methodology we use be compatible with the commercially available Emotiv EPOC EEG-headset, which has considerably less electrodes than the EEGs used for medical applications, and will thus indirectly give clues whether or not the methodology used is capable of detecting emotions with equipment anyone can get their hands on.

During the exploration of BCI systems, we found that many of the systems were based on a large variety of features extracted from the EEG signal of subjects. Some of these were just simple measurements, while others were more sophisticated and advanced in nature, but all have in common that they were chosen by the creators of the systems because they are believed to give some meaningful descriptions of the data. Many of these may very well be highly descriptive, but we believe that it is possible to avoid this subjectivity (of choosing what methods to use in order to extract features) by using a method capable of generalizing over the nature of the problem as is. Avoiding features does also mean a reduction in the computational overhead they pose, which is important in systems that require a quick response.

Looking back to what EEG is makes it clear that we are dealing with signals that are read from different positions of the skull of a subject. This makes it a problem

that is geometrical in nature. A neuroevolutionary method called HyperNEAT that directly evolve solutions on the basis of the basic geometry of the problem is then our choice of method to evolve ANNs that are capable of detecting and outputting values encoding for different emotions, based on the model of emotions we rely on.

Our research question is then to *investigate if HyperNEAT is a viable technique for detecting emotions in EEG with the hardware limitations posed by the Emotiv EPOC headset, and by that find out if it is possible to avoid the subjectivity involved with choosing methods for feature extractions and the computational overhead they pose, as well as an indication of the commercial value and impact of our system.*

The structure of the thesis is as follows. This chapter will gives a brief introduction to the problem areas, our motivation for this specific problem, and our research question.

Chapter 2, Background, starts with exploring different models and notions of emotions, followed by an introduction to EEG and common computational methods used in EEG analysis. We then give an introduction to BCI and commonly used methods for BCIs in general and for emotion recognition. Lastly comes an introduction to neuroevolution and a detailed explanation of the HyperNEAT method, and where it stem from.

Chapter 3 is called Implementation and Methodology, where we first get familiar with the EEG signal, followed by a description of how we implemented HyperNEAT, a brief test of the capabilities of the implementation, and finally the formal configuration of our model.

Chapter 4, Experimental Results and Discussion, presents our experiment and displays the quantitative results, followed by a qualitative investigation in order to highlight interesting findings in the results.

Chapter 5, Conclusion and Future Work, is the concluding chapter of this thesis where our formal conclusion appears along with comments on limitations and future work.

Chapter 2

Background

Psychology, neurophysics, neuropsychology, physics, and computer science, are all part of the multidisciplinary approach to this thesis. More specifically: Emotions, electroencephalography (EEG), neuroevolution (NE), brain computer interfaces (BCI), affective computing, and intelligent user interfaces (IUI), are all subjects or fields that influence and motivate this work to such an extent that we feel that it is necessary to present them, both from a scientific and philosophically point of view, to the reader before venturing into the main chapters.

This chapter will serve as a theoretical background, projecting our justification for the methodology chosen and our motivation for investigating this highly challenging problem—why we find this particular research area important in general. By tying together the previous mentioned fields and topics, alongside an analysis of related work which we consider important or state of the art, an overview of the problem area arises, which do elicit our research question as posed in Chapter 1.

2.1 Emotions

What are emotions and mood? –This question, when generalizing in to the broad term affect, has intrigued mankind ever since the ancient philosophers, and probably even earlier, if one consider a general increase in self-consciousness alongside the evolutionary increase in the intelligence of humans. It is however hard to document these early thoughts on affect—a cave painting may display affective states, but it is surly unclear if those paintings merely displays affective states as experienced by the painter, or if they display the painter's self-conscious thought on the experience of the states. We will thus focus on well documented (written), and hence work

on affect and emotions which are easily referenceable when deducting a notion of emotions to rely on in this thesis.

Aristotle was one of these early philosophers with clear ideas about emotion, and wrote in *Rhetoric* (1378b, English translation by W. Rhys Roberts):

> "The Emotions are all those feelings that so change men as to affect their judgements, and that are also attended by pain or pleasure. Such are anger, pity, fear and the like, with their opposites."

This statement itself is not unproblematic, as discussed in (Leighton, 1982), but more interestingly in this context: he identifies (even ever so vaguely) distinct emotions (anger, pity, and fear) as emotions felt by human beings. No such distinct emotions are mentioned in the *Republic* of Plato. However, the emotive part seems to be one of his three basic components of the human mind, while Aristotle on the other hand had no such vision of a separate module of mind, but did instead see emotions as important when it comes to moral (De Sousa, 2012). Descartes, with his dualism (separation of mind and body, which occasionally meets in a gland at the stem of the brain), refers to emotions as a type of "passion", where his six "primitive" passions are: love, hatred, joy, sadness, desire, and wonder (Solomon, 2010). The gland he referred to was the "communication point" of mind and body, allowing bodily manifestation of passions (emotions) and vice versa, which helped keeping his theory of dualism valid.

It is evident that all the great thinkers had their unique theories on emotions. Some thin lines could be drawn between Aristotle's distinct emotions and Descartes's primitive passions, if one is ignorant on their different perspectives on mind and body—where emotions stem from, what they are in the realm of the human mind, and how they manifest. Even the meaning of the words "emotion" and "passion" have changed sufficiently through millennia and centuries, and thus contributing further to the uncertainty regarding early affective studies and how to compare them to each other (Solomon, 2010).

It is also evident, by reading modern research, that these great thinkers should not have their theories on emotions completely discarded; some of their insight is still valid. The invalid theories just prove the difficulties in trying to understand, and model, human emotions. Some of these difficulties may have a generational origin, that is, the overall focus of the creator of the theory seem to be heavily influenced by the areas that the society in general was concerned with (e.g. different views on morale and ethics). Another generational issue is the limitations posed by the scientific progress in other research fields. A good example of this is Descartes with

his slightly confused view of the actual functions of the pineal gland, which was by that generational standard, based on state of the art science on human anatomy (Solomon, 2010).

The other main ingredient in the soup of uncertainty of human emotions is naturally subjectivity. An emotion is indeed a subjective experience, and the ability to communicate an emotional state to others is severely limited by the subject's physiological and psychological capabilities, previous experiences, and the uncertainty about the code used to communicate (e.g. the actual meaning of a written or spoken word). Unfortunately, creating a model of emotions which is generalizable to most in the total human population requires self-reported data (possibly lots of it), given the complexity of the problem. Considering the previous mentioned causes of uncertainty in self-reported data, it is clear that a perfectly reasonable model of emotions may suffer badly in terms of accuracy and generalizability just because of the variance introduced by this uncertainty. More precisely: a sound model might be falsely rejected because of uncertainty in self-reported data that is not accounted for.

Psychology—the science of mind—base its research, and thus its universal theories of the human mind, on observed or self-reported data. As emotions receive a constant attention in psychology, constant attempts have been made to identify a universal notion of emotions which accounts for the variance in self-reported data on affect, and hence reducing the uncertainty of the data itself. The basis for psychological research (or any types of research) on emotions is lost without a universal notion of emotion; research without sufficient statistical power have in best cases only a weak influence on its field (or any field) in modern science.

Motivated by an interest for an adjective check list for self-report data on mood, Nowlis and Nowlis (1956) conducted factor-analysis on data gathered from subjects, in a quest for some independent factors of mood. As shown in (Russell, 1980), this triggered a relatively large group of psychologist to conduct similar studies, where all concluded with 6 to 12 independent mono-polar independent factors of affect. As an example of these factors, Russell (1980) lists the following of what this group found: the degree of anxiety, tension, anger, sadness and elation. This is an important step in the attempt to create a notion of emotion which accounts for the variance in the self-reported data—it is the beginning of the theory of discrete categories of emotions, and its underlying assumption (Russell, 1980).

Paul Ekman, inspired by Darwin, did in his cross-cultural work on universal facial expressions, find six basic emotions: anger, disgust, happiness, sadness, surprise

and fear (Ekman and Friesen, 1971), where disgust and surprise are debated as too simple to be called emotions (De Sousa, 2012). Ekman did in (1992) state: "It should be clear by now that I do not allow for "non-basic" emotions", yet later he proposed in (Ekman, 1999) an extended list of 15 "emotion families" which could by his definition be thought of as basic. This could be an example of challenges met when dealing discrete categories of emotions, and leads to the following questions about this notion: do the labels (words) change over time, and if they do change over time, how can one be sure that the labels used are valid as per now? Another important question is: are all or most emotions basic, and if they are, would not the universal labels of the basic emotions just capture a consensus of the meaning of the few labels listed as basic by Ekman and likes? We will not attempt to answer these questions, but we do identify them as important ones regarding this notion. Anyhow, discrete categories of emotions do provide a statistical sound notion of emotions which account for some of the variance in self-reported data on affect, even though the number of categories/labels may restrict the resolution and share number of universal emotions.

Interestingly, alongside this notion exists the notion that emotions are better described by a few dependent bi-polar dimensions, than by a range of independent mono-polar factors. Schlosberg presented a three-dimensional model of affect: sleep-tension, attention-rejection and pleasantness-unpleasantness (Schlosberg, 1952, 1954). Inspired by this model, Russell (1980) presented his two-dimensional circumplex model of affect. The first of the two dimensions are pleasure-displeasure, which is analogous to Schlosberg's pleasantness-unpleasantness. The second, arousal-sleep, is a combination of the other two dimensions in Schlosberg's model, as Russell in his work found the two of them so correlated (r=.85) and therefore not differentiable (Russell, 1980). Even more valuable than a reduction of dimensions, he discovered that the model accounted for much of the variance in self-reported data, which makes the model quite robust. Conte and Plutchik's work on a circumplex model of personality traits (Conte and Plutchik, 1981), and Plutchik's later "wheel of emotion" or "solid of emotion" (Plutchik, 2000, 2001) does further support this notion of emotions.

We will rely on this notion through this thesis, and target Russell's model when considering test-data and classification. That is, using his model as a metric for emotions. The model itself is based on the internal representation of affect of the persons tested, their cognitive structure of the interpretation of emotions, and not a description of their current affective state (Russell, 1980). A universal and easily transferable metric is then achieved, compared to a metric from the notion of some

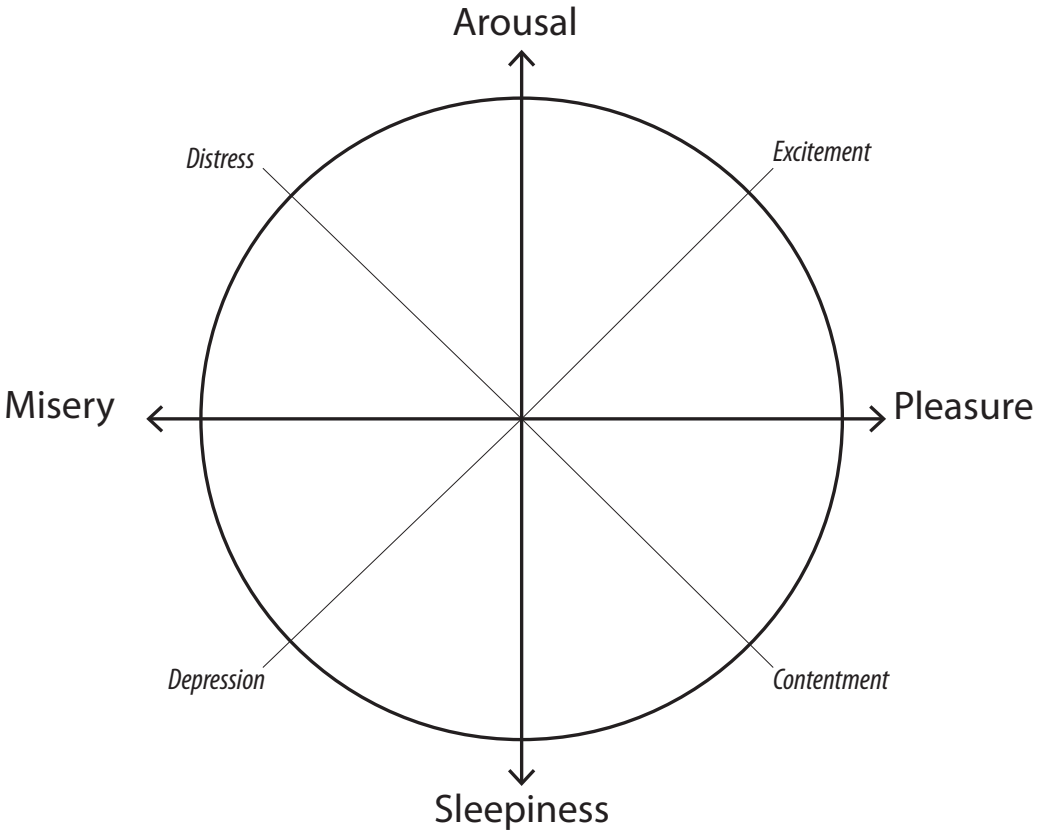

Figure 2.1: The two dimensional notion of emotions we rely on in this thesis (from Russell, 1980)

specialized mono-polar factors.

Going back to the great thinkers, it is easy to unveil their insight and their influence on the research on emotions. Descartes with his primitive passions are much in line with the notion of mono-polar discrete factors of emotions, even though the exact meaning of the labels (words) is unclear. Aristotle's statement about emotions could actually be interpreted as valid to both notions; he lists a few distinct emotions on the one hand, but on the other hand he does end the statement about emotions rather open. By open, we mean that is unclear whether or not the opposites of the emotions mentioned was independent mono-polar factors, or just at the other end of a dependent bi-polar dimension. This will remain unanswered.

2.2 A Window On The Mind

By calling Electroencephalography (EEG) for "a window on the mind", Nunez and Srinivasan (2006) captures the essentials of what EEG is: a "window" invented by Hans Berger in 1924, which allow us to take a closer look of what is really going on inside a brain.

The window is created by attaching electrodes at different positions on the scalp of the subject which reveals the mesoscopic (in the world of neurons) regional difference in electric potentials. Assuming that different cognitive patterns create unique activation patterns makes the oscillating signal from the electrodes the electric manifestation of our brain activity, and thus to some degree our mind. However, as with a house and its windows, EEG is limited by the density (spacing between) of electrodes; it is easier to get the correct picture of what is inside a greenhouse, than it is with a bunker. Another important factor is the placement of the electrodes on the scalp. If we consider a range of subjects to have their EEG recorded for a definite time window, then the recordings would be practically useless when comparing results, if the electrodes were placed at random.

In an attempt to reduce the uncertainty of what (as a result of where) that is being measured, a standard called the "10-20 system" was introduced (Malmivuo and Plonsey, 1995). This is the current working electrode placement system when recording EEG signals on human beings, and takes its basis on universal landmarks on the human skull (nasion and inion). The "10-20" in the name, indicates that the first electrode placed should be separated from the landmark with a distance of 1/10 of the total distance from one landmark to the other, while the rest of the electrodes should be separated by 1/5 of the total distance. Each electrode in this system got a unique id which is a combination of characters and numbers, where the characters encodes for the specific region (lobe) of the brain, and the number encodes for the specific position on that particular lobe. The numbers do also indicate on which part of the right/left homologues hemispheres of the brain an electrode is located, where even numbers encode for right hemisphere and odd numbers encode for left hemisphere.

As pointed out earlier, and by Nunez and Srinivasan (2007), researchers do often want to achieve as high as possible resolution, and thereby density, of the electrodes when collecting data. This has led to extended versions of the 10-20 system, like the 10% system proposed by the American Electroencephalographic Society (AES) (Sharbrough et al., 1991). This system, with its increased resolution, follows the basic principles from the 10-20 system both in approach and in the naming convention

of the electrodes. Few direct conflicts exist between these systems, so it is possible to compare the result between the two of them. The choice of which of the systems to use, do often come naturally by the number of electrodes available, as they both achieve the same by using the same technique: relative positioning of the electrodes which minimizes the variance in the data from different recordings, from possibly different subjects with different skull shapes.

We will rely on the 10-20 system in this thesis, since both our EEG setup and data do so.

So with an idea of what EEG is, and how electrode placement systems allow quantitative research by creating a similar "window on the mind", it is time to investigate some commonly used computational methods which gives meaning to the oscillating signal received from the electrodes. Nunez and Srinivasan (2007) provides an excellent overview, starting with some basic signal processing.

$$V(t) = \sum_{n=1}^{N} A_n \sin(2\pi f_n t - \phi_n). \tag{2.1}$$

Equation 2.1 shows the nature of an EEG signal (or any physical waveform), and stems from the theory that a signal in the time domain can be described as a Fourier Series, that is, a sum of its different three components (phase ϕ, frequency f and amplitude A) (Nunez and Srinivasan, 2007). From this theory rises the most commonly used computational method to analyse EEG, namely spectral analysis.

$$X_k = \sum_{n=0}^{N-1} x_n e^{-i2\pi k \frac{n}{N}} \quad k = 0, \ldots, N-1. \tag{2.2}$$

A composite EEG signal $V_m(t)$ in the time domain, where m indicates the electrode pair, can be transformed into the frequency domain and its respective components by performing a Fourier transform. The most commonly used Fourier transform is a Fast Fourier transform (FFT), which could be one of many efficient implementations of the discrete Fourier transform (DFT), and is formally defined in equation 2.2. One of these algorithms is the much used Cooley-Tukey FFT algorithm which reduces the computation time of DFT from O(N^2) to O($NlogN$), a speed increase which is hugely important when dealing with massive datasets or creating a (near) real-time system (Cooley and Tukey, 1965).

The result from a Fourier-transformation of an EEG signal in time-domain is a set of frequency coefficients X, where $|X|$ is the amplitude spectrum as illustrated in figure 2.2, and X^2 is the power spectrum. From these spectrums, one may identify

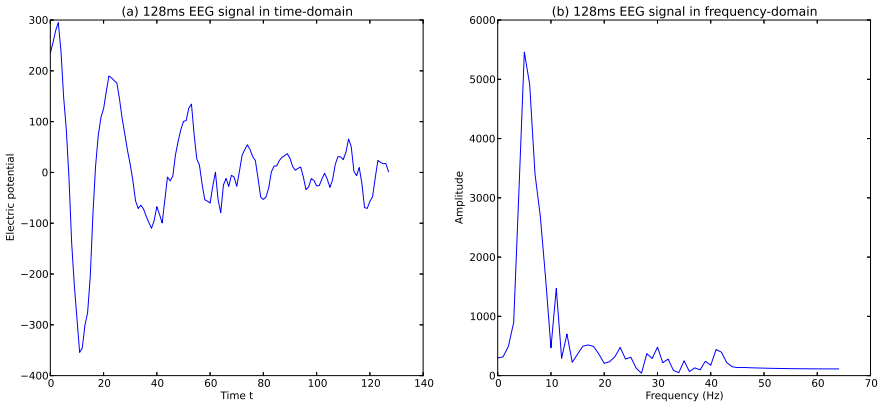

Figure 2.2: A 128 data point EEG in the time domain (a), and the same signal in the frequency domain (b). The Cooley-Tukey algorithm with $N = 128$ is used to transform the signal

the typical EEG-ranges (bands) used for analysis: delta (0–4 Hz), theta (4–8 Hz), alpha (8–13 Hz), beta (13–20 Hz) and potentially gamma (30–40+ Hz) (Nunez and Srinivasan, 2006). We say "typical" about these infamous bands, because, as pointed out by Nunez and Srinivasan (2007), unique combinations of these bands are found to encode for cognitive states, behaviour, location on the brain, and so forth. In other words, combinations of these bands do seem to encode for interesting psychological and physiological (neurological) phenomena.

Rather than just accepting this as a computational method that clearly works, we want to explore the obvious questions: (a) from where do these qualitative labels have their origin, and; (b) why is it such that a (potential) loss of information and precision is preferred to the output from the transformation as it is?

The answer to (a) lies in the history of EEG from when it was printed out continuously on paper, and experts in interpreting the print manually counted zero-crossings within a given time interval, where the ranges served as qualitative labels (Klonowski, 2009; Nunez and Srinivasan, 2006). An answer to (b) is however not so simple but may be explained as a result of the nature of the EEG signal and how it is transformed.

From Klonowski (2009) and Sanei and Chambers (2008), we have that an EEG signal, and many bio-signals in general, is described by the "3 Ns" (noisy, non-linear, and non-stationary)[1]. Klonowski argues that many researchers do agree that the human brain is one of the most complex systems known to humans, and therefore

[1]A more detailed explanation of noise and artifacts in EEG, and how to automatically reduce them, can be found in (Kvaale, 2011)

treating it as a linear system seems unreasonable, which as an argument seems reasonable. As a side note, this highlight an interesting paradox—we know (or think we know) more of the universe as a highly complex system, than of the system (human brain) that is producing that knowledge.

Treating a non-linear system as linear will naturally not capture its dynamics correctly. Hence using linear methods like FFT, do in best case capture a simplified view of the dynamics in an EEG signal. While this sound unoptimistic, let us not forget that this simplified view is what the main portion of EEG research have been using with promising and statistically sound results. However, this only highlights a problem using linear methods, and provides no direct clue to (b).

A basic assumption for FFT is that the signal is stationary (no change in statistical distribution over time), which is clearly violated since EEG signals is non-stationary. The effect of this violation is clear in (Klonowski, 2009), where he illustrates this by applying FFT to a 12Hz signal with its amplitude modulated with 1 Hz, resulting in two harmonic signals of 11Hz and 13Hz with half the amplitude of the original 12Hz signal (fig. 2.3). This is where we might find a clue in an attempt to answer (b) and why research using this technique appears to get some valid findings, even though treating the system with a lower complexity than what it actually is (linear), and violates the basic assumptions of FFT (stationary). From the example, if one considers 11-13Hz as a band, then the sum of the band will be equal to the original 12Hz frequency, and does therefore yield the same result as if the signal was stationary, so the bands functions as "safety nets" for the non-stationarity. It is also evident that a smearing from neighbouring bands and frequencies will distort the total sum, adding uncertainty to the results, but is anyhow a better estimate than looking at the single 12Hz (which appear as zero).

The answer to (b) may then be that what appear to be the most descriptive ranges of EEG-signals, are actually the ranges where the smearing produced by the non-stationarity is of lowest variance, or where the borders of the ranges minimize overlapping, and hence providing the most stable results. So the ranges are actually the most descriptive ranges of the EEG-signal *with regards to linear, and possibly stationary, time-frequency transformation methods.* Although a loss in precision is inevitable (what is the exact frequency coeffecient?), one must say that this computational method is a perfect example of where a naïve approach to a system with an unknown scale of complexity, is producing viable results, and thus making headway in the general knowledge of the system itself.

Researchers like Klonowski (2007, 2009), Nunez and Srinivasan (2007) and Nunez

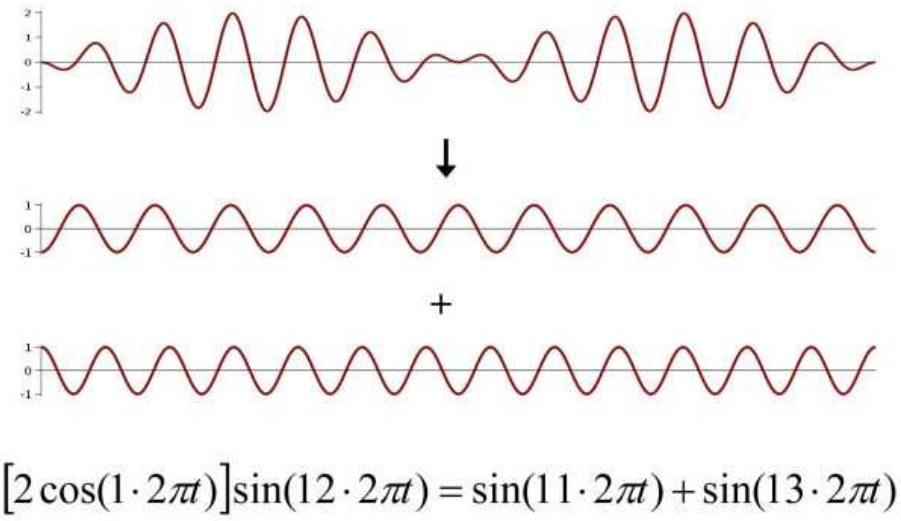

Figure 2.3: A 12Hz signal with its amplitude modulated by 1Hz results in two harmonic waves of half the amplitude, when transformed with FFT, because of the violation of the basic assumption that the signal is stationary (from Klonowski (2009)).

and Srinivasan (2006) do all indicate that EEG research on non-linear and dynamic systems will contribute to an increase in our general understanding of brain function, and its physical aspects. Dynamic behaviour of sources (brain dynamics) and brain volume conduction are mentioned as computational methods in EEG by (Nunez and Srinivasan, 2007), and they are essentially the study of the physical aspects of EEG. The study of brain dynamics is concerned with the understanding and the development of models that correctly describes the time-dependent behaviour of brain current sources (e.g. the propagation speed in brain tissue, interaction between hierarchical, local and global networks, frequency dependence, resonant interactions, and so forth)(Nunez and Srinivasan, 2007). Many plausible mathematical theories have been proposed regarding brain dynamics that helps in the understanding at a conceptual level, but a comprehensive theory on the subject is yet to be developed (Nunez and Srinivasan, 2007). Brain volume conduction is on the other hand concerned with the relationship between the brain current sources and scalp potentials, and how the fundamental laws of volume conduction are applied to this non-trivial environment of inhomogeneous media (Nunez and Srinivasan, 2006). It is thus directly linked to the *forward problem* and the *inverse problem* in EEG, which is the problem of modelling and reconstruction of the underlying brain current sources, respectively. The laws of brain volume conduction do by its idea of linear superposition allow for a vast simplification in EEG, and is like stated in (Nunez and Srinivasan, 2006) *one dry island in the sea of brain ignorance. It should be treasured in a manner similar to Reynolds number in fluid mechanics.*

2.3 The Brain and The Computer

Where the invention of EEG opened up a window on the mind, the increase in computational power from computers and digitization of EEG and other technologies which measure brain activity, led to a new type of human-computer interaction—Brain-computer interfaces (BCI). The first use of the term BCI as a description for an interface between brain activity and a computer can be traced back to 1970 and Jacques Vidal, when he proposed a system trained on a triggered change in the recorded electric potential from subjects, when presented with visual stimuli (McFarland and Wolpaw, 2011). A diamond shaped board with flashing lights in each corner was the stimuli presented, where the distinct change in electric potential from looking at the different corners represented up, down, left and right commands in a graphic maze navigation program.

This early example highlights a commonly used method in BCI: the analysis of evoked potentials (EP), that is, the analysis of the distinct waveform produced by the synchronous neural activity over a region, phase-locked to an external stimulus (McFarland and Wolpaw, 2011). Since the actual voltage of an EP might be low compared to the other on going activity or noise/artifacts, one typically has to repeat the same stimuli-event several times, and the averaging of all these events in the time-domain elicit the underlying EP. Different EPs are often referred to by what type of stimuli that triggered the potential (e.g visual evoked potential), and by their internal negative and positive components (P300 potential). These components are the actual peaks of the transient waveform, where P or N code for positive and negative peaks in voltage respectively, and the number following the letter is simply the elapsed time in milliseconds after the presented stimuli. A universal syntax and semantic like this, is essential for the progression of the fields dependent on evoked potentials, because it allows for direct comparing of similar studies, and has led to dictionaries of distinct EPs, and what different combinations of the temporal alignment and voltage of these distinct EPs encode for in terms of physiological and psychological properties of a subject when presented with a standardized stimuli (e.g. duration of a flashing light, from a certain angle). An example of this can be seen in figure 2.4 (b).

So since different stimuli produce slightly different waveforms, it is possible to exploit this by training a classifier to separate them, which is the essential theory behind BCI systems using EP.

Another commonly used technique in BCI is based on changes in sensorimotor rhythms (SMRs), where SMRs are rhythms in an EEG-signal as a result of move-

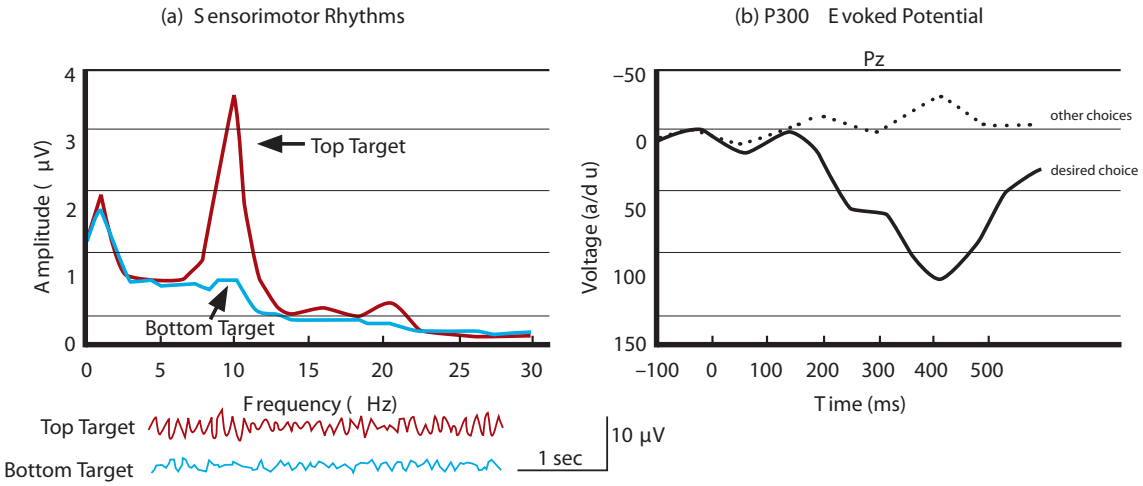

Figure 2.4: (a) Illustration of user-controlled change in the sensorimotor rhythms. (b) The result of different choices in stimuli in the p300 evoked potential. (Adapted from McFarland and Wolpaw, 2011)

ment, or even the thought of a movement, recorded over the sensorimotor cortex (McFarland and Wolpaw, 2011; Wolpaw et al., 2002). Spectral analysis, as previously mentioned, is used to identify such changes in the sensorimotor rhythm from subjects, and commands may therefore be mapped to distinct combinations in amplitude of the frequencies (see figure 2.4 (a)). Moreover, since a change of rhythm is registered even from an imagined movement, commands may be mapped to these imagined states of movement, and thus allowing for control of a system by spontaneous brain activity. The difference between the two different techniques mention so far is now clear: EP relies on changes in electric potential as a result of a stimuli, while SMR require no such stimuli and can be changed from the thought of a movement.

McFarland and Wolpaw (2011) do also point to their earlier study (Wolpaw et al., 1991) where subjects where trained to alter their SMRs in two distinct ways. These two distinct patterns were coupled with two commands, allowing the subjects to move a cursor in two dimensions. In Wolpaw et al. (2002) it is also clear that another studies used a similar technique which allowed subjects to answer yes or no to questions, and achieved an accuracy of $> 95\%$ (Wolpaw et al., 1998; Miner et al., 1998). No matter how amazing this is—the capability of altering our pattern of thought by concentration—the technology which utilizes and promotes such activities poses some serious ethical questions. Ros et al. (2010) did in their study find long term changes in subject's activation patterns to occur after as little of 30 minutes of self-controlled changes in brain rhythms. The implications of this self-imposed neuroplasticity is unknown, and questions about releasing products to-

day that rely on self-controlled brain rhythms commercially to the gaming marked, which is the biggest marked for BCI as of now, should be asked.

Even though invasive technologies exist (e.g. intra-cortical electrodes) that are suitable for BCIs, and research on this has found interesting topographic potentials useable in BCI systems (Levine et al., 1999; Wolpaw et al., 2002), it is clear that that more testing is needed to determine its effectiveness and what the long terms effect of having implants have on humans (McFarland and Wolpaw, 2011). We will thus not further explore this branch of BCI, for now, and leave it for future growth.

Conceptually, three types of BCI systems exist according to (McFarland and Wolpaw, 2011): (1) the system adapts to the user; (2) the user adapts to the system, and; (3) both user and system adapt to each other. Ideally would all BCIs be classified as the first, acting as the ultimate "mind reader", knowing when to function as a control and when to passively adjust what is presented to the user, or when to not do anything at all. Realistically, specialised systems are spread over all three categories. Systems monitoring cognitive states, medical conditions, or in some way silently gather information about the user, in order to produce a specialized output about/to the user, will I most cases go under the first category. If the BCI is to be used as a direct controlling interface for some hardware or software, then it will typically end up in the second or last category. A good example of this could be a thought of BCI system, which controls a mouse-cursors movement on a computer screen by change in gazing in two dimensions. It will be classified as the second category if the movement speed of the cursor was modulated by user training, and classified as the last category if the system itself recognized the user's desired movement speed.

EEG is by far the most common choice for BCI systems, but Van Erp et al. (2012) as well as McFarland and Wolpaw (2011) mentions the following as technology encountered in the literature of BCI research:

- electrocorticography (ECoG)
- intracortical electodes (ICE)
- functional near-infrared spectroscopy (fNIRS)
- functional magnetic resonance imaging (fMRI)
- magnetoencephalography (MEG)

All of these are however restricted to medical use or research, due to bulkiness (MEG), being intra-cranial (ECoG, ICE), or suffers from low temporal resolution

due to being an indirect measurement of activity (fNIRS, fMRI), where most of these technologies easily falls into several of these reasons. Future technology and advancements may however change this list completely, but until then, EEG stands out as the appropriate BCI for commercial and non-medical use (Van Erp et al., 2012).

Such facts do not go unnoticed by the industry, and has led to the development of cheaper and more portable EEG systems, possibly with high resolution, like Nurosky and Emotiv EPOC. The Emotiv EPOC headset is the targeted hardware of this model and consists of 14 electrodes, plus two electrodes used as reference, with standard placement according to the 10-20 system (see figure 2.5). Its sample rate is 128Hz (2048Hz internal) with a precision of 16bit. Digital notch filters is used to filter the frequency to a range of 0.2-45Hz, which makes the sample rate adequate according to the Nyquist frequency (critical frequency), and thus aliasing free after a discrete transformation. The headset itself is wirelessly connected to a computer by USB-dongle in the 2.4GHz band, so some degree of portability—freedom for users to move around as they want—is achieved (few meters). Although this makes the headset less intrusive to a user compared to a traditional wired EEG system, it may contribute to an increase in artifacts included in data recorded due to myogenic and oculogenic potentials, as well as the movement and friction of the electrode itself. This means that what is gained in data quality by the increased naturalness for the user when recording, might actually be lost in the increase of uncertainty about the signal. We cannot seem to find any direct studies on the relations between naturalness in the user environment and its effect on recorded data, and only a few indirect studies mentioning movement artifacts when using a wireless EEG (Gwin et al., 2010; Berka et al., 2004, e.g.). A conclusion to whether a wireless solution is a good or bad thing, in terms of naturalness of brain rhythms versus increase in unwanted signal, is therefore not possible. One thing however, that is certainly for sure, is that people tends to behave unnaturally in unnaturally environments, leaving a minimally intrusive interface as the best choice.

The new inexpensive and commercially available EEG systems, in our case Emotiv EPOC, makes research on EEG based BCI systems much more available as minimal funding is required to get started, and the result is a more than linear growth in publications with a great variety of focus areas and methods, such as the system proposed by Dan and Robert (2011) that uses Emotiv EPOC to control a Parallax Scibbler[2] robot. They recorded 10 seconds time frames, where a subject blinked its eyes, and presented these cases to a two-layer neural network with a training

[2] Parallax Scribler: http://www.parallax.com/tabid/455/Default.aspx

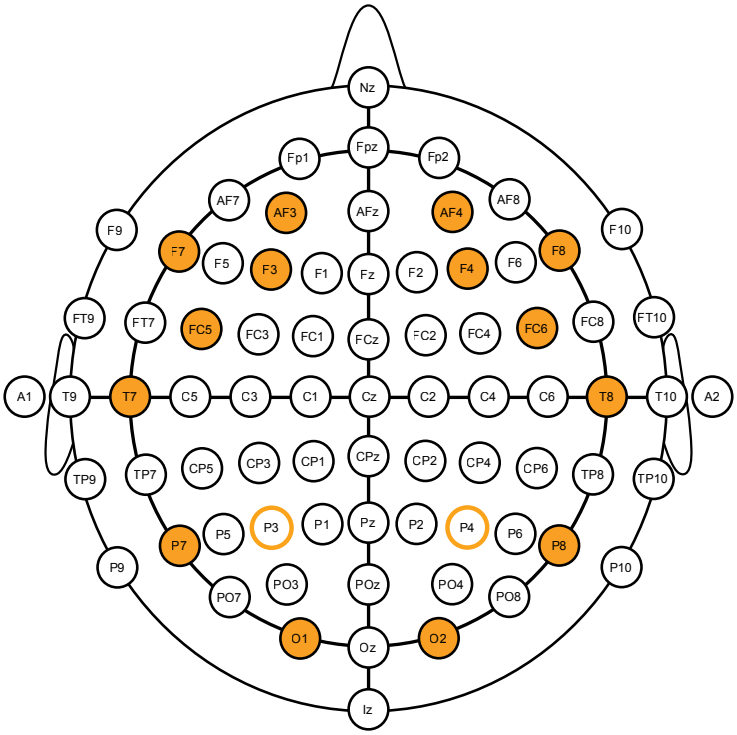

Figure 2.5: The solid orange electrodes is the available electrodes in the Emotiv EPOC headset, with positions and labels from the 10-20 system. The orange circles are the reference nodes.

accuracy of 65%. It should be noted that they only used one channel, because visual inspection of the cases revealed that it was the channel with the highest change in amplitude following a blink. A 100% training accuracy was achieved by further reduce the 10 second windows down to 1.60 seconds to minimize the effect of the temporal alignment of the blinks. One has to question whether this is a "real" BCI or not; EPOC does easily pick up strong myogenic potentials from its front sensors, which then makes this system an electromyography (EMG) based interface. Nevertheless, the system is a clever use of technology which require little to no training to operate, even though it based on strong artifacts in the world of EEG.

Another example is Juan Manuel et al. (2011), who do in their Adaptive Neurofuzzy Inference System (ANFIS) based system reveals that the P300 evoked potential can successfully be detected by using EPOC. In their experimental setup, the P300 EP is triggered on subjects using visual stimuli, and the data recorded was pre-processed and classified by the ANFIS with 85% accuracy (65% when accounting for false positive). The pre-processing in this system is quite substantial as it first involves band pass filtering, then blind source separation (independent component analysis), and last a discrete wavelet transform in order to decompose the signal. The ANFIS itself is quite interesting, as it combines a Sugeno-type sys-

tem with four linguistic variables and an artificial neural network trained by hybrid learning (back-propagation and least-square) to approximate the parameters in the membership functions.

The P300 EP is also successfully detected by the system presented by Grierson (2011). Unlike (Juan Manuel et al., 2011), they use the low-resolution Neurosky Mindset headset in their experiments, where subjects were presented with visual stimuli to trigger the EP. Traditional averaging of many similar time frames is performe in order to elicit the underlying waveforms, which is then used to train a simple linear classifier based on the area under the distinct curves. An accuracy of 78.5% is achieved when trained on two different stimuli (blue circle and red square).

While we could have extended this list of illustrative and interesting BCI systems using commercially available EEG headset with great success, we will now turn our focus to BCI systems that involves detection of emotions through EEG, since our overall goal is to be able to do so. This overall goal is motivated by the fact that machines do not incorporate live human emotions in their principles of rationality, even though they play and important role in modulating human rationality, and is thus to some degree a part of the definition of human rationality which makes us capable of behaving intelligently, especially when interacting with other humans. We believe that most have experienced the rationality mismatch between machines that do not incorporate human emotions in their principles of rationality and humans, which is illustrated with an example in Chapter 1. Another example could be automated advertising solutions in online newspapers, where an ad typically appears next to an article about the same basic topic as the product in the ad. The unwanted behaviour from the machine here, is when it matches an ad and an article that is about the same topics, but is together found totally inappropriate. We recently saw an example of this, where an article about hundreds of stranded dolphins was matched with an ad for frozen fish. There is no wonder why both the consumer and the company see this as unwanted behaviour from the machine.

If we look at the definition of Intelligent user interfaces by Maybury (1999), stating that *Intelligent user interfaces (IUI) are human-machine interfaces that aim to improve the efficiency, effectiveness, and naturalness of human-machine interaction by representing, reasoning, and acting on models of the user, domain, task, discourse, and media (e.g., graphics, natural language, gesture)*, it is quite clear that affective computing and the recognition of human emotions can contribute in achieving those goals.

We will now describe BCI systems that aim to detect human emotions in EEG,

starting with Sourina and Liu (2011) who proposes as system for emotion recognition by the use of Support Vector Machine (SVM) trained on features extracted from EEG recordings using Fractional Dimension (FD). Their hardware setup was the Emotiv EPOC headset, which they used to record the EEG of 10 and 12 participants while they listened to audio stimuli thought to elicit emotions. This was done in two different recordings, where the first was segments of music that was labelled by other subjects than the actual participants, and the second used sound clips from the International Affective Digitized Sounds[3] (IADS) that comes with normative ratings for each clip. The four classes of emotions they use are the four quadrants in the two-dimensional model of emotion (arousal-valence), and were gathered from the participants using the self-assessment mannequin (SAM) after each clip.

The pre-processing of the signal is a 2-42Hz band-pass filter, and the features was extracted from each recording using both the Higuachi Algorithm and the Box-counting Algorithm, on a 99% overlapping 1024 data point sliding window. This was however only done for three of the electrodes (Af3, F4 and Fc6), where they used Fc6 for the arousal dimension, and Af3 and F4 for the arousal dimension. By training the SVM on randomly selected 50% of the cases per subject, and testing on the other half, they report a performance of 100% on the best subject(s), and around 70% on the worst, where both of the feature extraction algorithms performed almost equally.

Petersen et al. (2011) uses features extracted by Independent Component Analysis (ICA), and the K-means algorithm, to distinguish emotions in EEG. Their hardware setup was the Emotiv EPOC headset, which was used to record the event related potential (ERP) in 8 subjects when viewing a randomized list of 60 images from the international affective picture system[4] (IAPS). These 60 images come with a normative rating which indicates how pleasant or unpleasant they are, or if they are rated as neutral. The set of 60 images used, is a perfectly balanced set with 20 pictures from each class. A repeated one-way ANOVA analysis revealed that the difference seen in the averaged ERPs is statistically significant ($p < 0.05$) in the P7 and F8 electrodes, which shows that their method are able to correctly distinguish between active and neutral images, as well as unpleasant and pleasant images. They further find that clustering the ICA components based power spectrum and scalp maps, revealed four distinct clusters which was completely covered by 3 standard deviations from their respective centroids, which gives an indication of the consistency in correctly identifying different activation patterns.

[3]IADS: http://csea.phhp.ufl.edu/media.html#midmedia.html
[4]IAPS: http://csea.phhp.ufl.edu/media.html#topmedia

As an interesting touch, they couple the Emotiv EPOC headset with a smart phone. They also implement a client-server model where the phone is the client and a standard PC is the server. This allow them to estimate and reconstruct the underlying sources in the EEG signal on the server side, and present them on a realistic 3d head model on the smartphone. The estimated activation plots on the 3d head model, from the ERPs when viewing the IAPS images, was found consistent with previous findings in neuroimaging.

Horlings et al. (2008) investigates the use of the naïve Bayes classifier, SVM, and ANN to detect different emotions in EEG. The hardware setup used in this study is the Deymed Truscan32[5] diagnostic EEG system that supports 24–128 electrodes. They recorded the EEG from 10 participants when viewing 54 selected pictures from the IAPS database, where each trail was followed by a self-assessment by the use of SAM and the two-dimensional model of emotions. From each sample, the frequency band power was measured along with the cross-correlation between EEG band powers, the peak frequencies in the alpha band, and the Hjorth parameters (Hjorth, 1970). A vast amount of 114 features per sample was the result of this extraction, where 40 of these were selected as the most relevant by the max relevance min redundancy algorithm. They report a 100% and 93% training accuracy for valence and arousal respectively, and a testing accuracy of 31% and 32%, for the SVM classifier. The neural network had a testing accuracy of 31% and 28%, while the naïve Bayes had an accuracy of 29% and 35%, so it is hard to conclude on what is the definite best classifier from the results. However, when manually removing potentially ambiguous cases located near a neutral emotional state from their set, they achieved an accuracy of 71% and 81% when testing the SVM. The reason for this behaviour is of course less need for robustness from the classifier, but the underlying cause of why these cases creates ambiguity is more intricate and may stem from the images seen, the EEG recordings, or because of the nature of the features extracted.

Mustafa et al. (2011) proposes a system that uses an ANN to detect levels of brain-asymmetry in EEG. While brain-asymmetry is not directly related to emotions, they are found to give an indication of schizophrenia, dyslexia, language capabilities and other motoric and mental phenomenon (Toga and Thompson, 2003), and the methodology used here show one way of detecting distinct patterns in brain activity in EGG by ANN. Their hardware setup was an EEG with two electrodes (Fp1 and Fp2), which they used to record samples from 51 volunteers, which was

[5]Truscan: http://www.deymed.com/neurofeedback/truscan/specifications

classified by the use of the Brain-dominance Questionnaire[6]. Spectrograms from these samples was then created using short time Fourier transform, and Grey Level Co-occurrence Matrices (GLCMs)(Haralick et al., 1973) in four orientations was computed based on these spectrograms. A range of 20 different features from these four GLCMs per recording was then computed, and the best 8 features from these 80 features was selected based on eigenvalue of components outputted by Principal Component Analysis. The ANN which had 8 input nodes, 6 hidden nodes and one output node was then trained on the training cases to 98.3% accuracy which gives indication that this methodology is capable of detecting distinct patterns in EEG.

Khosrowabadi et al. (2010) proposes a system for recognition of emotion in EEG, based on self-organizing map (SOM) and the k-nearest neighbour (k-nn) classifier. Their hardware setup was an 8 channel device, which was used to record the EEG of 31 subjects who listened to music that is thought to elicit emotions, simultaneous to looking at different pictures from the IAPS dataset. A self-assessment by the use of SAM was used after each trail in order to classify the recording in four different classes. These samples was then processed with a band-pass filter to exclude frequencies above 35Hz, and features was then extracted by the magnitude squared coherence estimate (MSCE) between all permutations of pairs of electrodes from the 8 available electrodes. The SOM was then used to create boundaries between the different classes based on the features extracted and the SAM scores, and the result from the SOM was then used by the k-nn to classify the recordings. Testing with 5-fold cross-validation revealed an accuracy of 84.5%, which is a good indication of the systems abilities to correctly distinguish between the four distinct emotions in EEG.

We can clearly identify a process in how the systems described typically approach the problem of detecting emotions or distinct patterns in EEG. The first step is to pre-process and extract features from the recorded signal, possibly followed by a reduction of features based on measurements of their relevancy. The second step is to train the chosen method for classification based on the features extracted for each subject and recording. This process is also seen in systems investigated in our preliminary studies (Kvaale, 2011). The act of choosing what methods to use in order to extract features depends on a subjective opinion of what the most descriptive features are, which clearly is disputed based on the variety of different features seen. Looking back at the actual nature of EEG (oscillating signal), and how it is recorded (electrodes at distinct position on the skull), reveals that it is indeed a geometrical problem. We want to investigate if it is possible to minimize

[6] http://www.learningpaths.org/questionnaires/lrquest/lrquest.htm

the subjectivity involved with extensive feature extraction, and thereby also the computational overhead they pose, by using the spatial information encoded in multi-channel directly, and let a method proven to perform well on geometrical problems generalize over this information. In other words, use a method more in line with the nature of the problem. We find such a method in the next section.

2.4 Neuroevolution

Traditional ANNs, with a hardwired structure and its weights learned by backpropagation, may perform excellent on a specific problem. However, if the problem changes its characteristics ever so slightly, then the previous excellent performance is likely to not be so excellent anymore. Another serious shortcoming of traditional ANNs learned by gradient descent is the scaling problem, that is, an increased complexity in input data results in in a loss in accuracy. Montana and Davis (1989) explains this phenomenon by pointing to the obvious shortcomings in gradient based search; it easily gets trapped in local minima. Motivated by this fact, they designed the first system that finds the weights of ANNs by an evolutionary algorithm (EA), which tends to more easily avoid local minima, and thus giving birth to neuroevolution.

A lot of different systems, with different complexity, have been proposed since then: Miller et al. (1989) proposed a system that used a genetic algorithm to evolve the connection topology for a neural network, followed by training (weight adjustment) by backpropagation. A similar approach is found in (Kitano, 1990) who also evolved the connection topology by evolution, and trained weights by backpropagation. A difference between these systems can be seen in their genotype encoding, where Miller et al. used a direct encoding (a complete connection table), and Kitano used grammatical rules to create a phenotype from a genotype. It is clear what is preferable in terms of scalability and modularity. Gruau et al. (1996) used evolution to find both topology (connections and nodes), and weights of the connections using cellular encoding. This encoding is also based on grammatical rules, but in this case for cellular division, or more precisely, the effects a cellular division has on topology and weights. Their results where impressive, and the system solved a pole-balancing problem that fixed topology networks was unable to solve, thus arguing for that evolving the structure was essential in solving difficult problems. Gomez and Miikkulainen (1999) did however solve the same problem with a fixed topology with their system called Enforced Sub-population, resulting in an inconclusive answer to what is better.

Another challenge in NE is the permutation problem (competing conventions problem), as pointed out in (Floreano et al., 2008; Stanley and Miikkulainen, 2002a). As the name suggest, this involves permutation of individuals in a population—how different genotypes that results in different phenotypes, may produce similar outputs. The problem arrives when two such individuals are selected for reproduction by the EA, and a crossover operator mixes their genes when producing offspring, resulting in a new individual with considerably lower fitness than its parents. This happens because of a too big a distance in solution space, resulting in crossover of genes that are not meaningful given the appearance of the parents, and thus low heritability.

NeuroEvolution of Augmenting Topologies (NEAT), as presented by Stanley and Miikkulainen (2002b,a), addresses both these issues. It is designed to increase the performance of NE by evolving both weights and topology, increase the heritability by addressing the permutation problem, and doing so with a minimized number of nodes and connections.

The genome encoding in NEAT is direct, and consists of node genes and connection genes. Node genes does simply specify available nodes that can used either as sensors (input nodes), hidden nodes, or output nodes. Connection genes specify the connection topology of the network, where each gene includes a reference to both pre and post-synaptic nodes, its connection weight, a bit indicator used to enable and disable connections, and its innovation number. The innovations number is a clever trick in NEAT to prevent the permutation problem. Each time a mutation occurs that changes the structure of the network, and thus the appearance of new genes, a global innovation number is incremented and assigned to these new genes. This number is never changed after it is first set, and do even persist when reproduction combines two parent's genes, by the rules of the crossover operator, in an offspring. NEAT will hence always have a chronological list of all genes in the system, which results in meaningful crossovers of genes, and thus good heritability.

Like mentioned earlier, NEAT is designed to minimize the network topology. By starting with a minimally complex network (in terms of number of nodes and connections), the system is allowed to effectively explore a gradually larger search space by introducing new genes through mutations, and ends up with an efficient structure that approximate the correct behaviour for a given problem. However, this bias towards less complexity, by starting minimally, poses a problem compared to systems that starts with an arbitrary topology size. It is easier for an arbitrarily large structure to remove excess nodes in order to maximize fitness, than it is for a minimal structure to add un-optimized connections or nodes that might in many

cases cause a temporary loss in fitness. Many mutations that eventually would have led to a better approximation of the behaviour, if allowed to be optimized over a few generations, may be lost due to a relatively too high selection pressure in Darwinian evolution (survival of the slightly fitter than the mutated individual).

NEAT counter this problem by speciation, where the global innovation number once again plays an important role. Instead of a tedious and inefficient comparison of actual topology, NEAT uses the global innovation number of the genes to line up a new individual with a random representative for a species. Their similarity is then computed according to the distance measure (equation 2.3), where E is the number of excess genes, D is the number of disjoint genes, and W is the average difference in connection weights. The importance of each of these variables can be adjusted by the c_1, c_2 and c_3 coefficients. If the distance δ is found to be under some given threshold, then two individuals compared are found to be the same species. This allows new individuals to compete for reproduction primarily with other similar individuals in terms of innovations, instead of competing with the entire population, which gives any new individual a better chance to survive until it has it newly mutated genes optimized.

$$\delta = \frac{c_1 E}{N} + \frac{c_2 D}{N} + c_3 \times W \tag{2.3}$$

To prevent early convergence, and hence a population totally dominated by one species, NEAT employs fitness sharing, which means that individuals within one specie must share the same fitness. This is implemented by dividing the raw fitness values of the individuals by the population size of the species that the individual belongs to. Then the amount of offspring to spawn is calculated by dividing the sum of all the adjusted fitness values within a species by the average fitness of the entire population. This means, in other words, that a single species will gradually lose their fitness as their population size increases, allowing new species and innovations to exist alongside possibly fitter species, and thus maintaining the overall diversity which is essential in evolution.

The main insight of NEAT is quite clear if we sum up the abilities of the method. First, the direct encoding with a global innovation number handles the problem of competing conventions, and hence ensures good heritability. Second, NEAT allow for incremental complexification by speciation, and does therefore explore the search space efficiently for the minimal topology needed to achieve the correct behaviour. Last, speciation does also play an important role in preventing premature convergence and thus maintaining diversity in the overall population. It is now clear that

it is the exploitation of the historical markings of genes that makes this NE system unique and light computational wise.

However, Stanley (2007) extends NEAT to produce what he calls Compositional Pattern Producing Networks (CPPNs) motivated by findings that suggests that developmental methods plays an important role in complexification in nature. This is intuitive; the human DNA is not a direct blueprint on how to construct a human, but instead an abstraction of the processes on how to do it. Like mentioned earlier, the human brain itself is argued as one of the most complex, if not the most complex, system known. If human DNA included a direct representation on how to create this system (e.g. the position of all neurons and how they are connected) along with the rest of the body, then it would be the utter most complex description known, which it is clearly not. The key is in the abstraction on how such developmental processes are encoded.

CPPNs are an attempt to create such a developmental encoding abstraction. Without regards to theory involved, then a CPPN is simply a network of connection and nodes, much like a traditional ANN. Its nodes however, deviate from typical ANN nodes. Where ANNs often use sigmoid or threshold activation functions, CPPNs may have activation functions that are symmetrical (Gaussian), periodical (sine and cosine), linear (scaled within a certain range) or any other simple function that makes sense given the properties of a specific problem area. The CPPN is then simply a compositional function, composed by the topology of the network itself. What this entails, with regards to encoding, is better explained by an example. The goal of the example is to write a character on a canvas in Cartesian coordinates. A direct encoding would have to explicitly store a value for each of the N x M points—a blueprint of the canvas and the character. An indirect encoding that relies on local interaction would have to store rules for the least complex possible way to describe the specified character and its temporal unfolding (from starting point to end point). CPPN on the other hand, uses only the coordinates of the canvas itself as input, and outputs the target character without the need for explicitly knowing how single points in space align, and when to draw them (local interaction and temporal unfoldment).

This is quite impressive; CPPNs draws a character given a canvas, and do by the geometry of the canvas implicitly know the local interactions and growth needed to create that character. A similarity to how people draw a character is present. Humans do not have to start at one end of a character to be able to correctly draw an approximation to a perfect version of that character (even though we often do due to the speed increase we gain trough enhanced motoric capabilities when repeating

the same motoric task over and over again). Also, humans do not have to measure, for example, the angle between different points on a canvas to be able to end up with the character we are to draw.

Built on the theory that a neural network with two hidden layers can approximate any function, where more complexity improves accuracy, Stanley (2007) gradually evolves CPPNs from minimal topology by using NEAT, and should thus in theory be able to approximate any compositional function. In a series of experiments in (Stanley, 2007) he shows that CPPNs evolved with NEAT are capable of displaying regularity, symmetry and repetition, which are thought to be essential in developmental encoding with regards to complexity of the phenotype, by using symmetric and periodic functions. Further, Stanley (2007) does also suggest that the spatial pattern produced by a CPPN encoding may be used as connectivity patterns for a 2 x 2 dimensional hypercube by allowing four inputs (two x and y pairs).

This is the origin to a method called HyperNEAT (Stanley et al., 2009; Gauci and Stanley, 2010), and is its main idea. Gauci and Stanley (2010) expresses this insight as concisely as possible: "2n-dimensional spatial patterns are isomorphic to connectivity patterns in n dimensions". This entails that regularities, symmetries and repetitions found in spatial patterns produced by CPPNs that uses the 2n-dimensional coordinates as inputs, is directly transferable if the spatial pattern is interpreted as a connectivity pattern for a 2n-dimensional hypercube, from which the coordinates inputted to the CPPN stem from.

CPPNs evolved by NEAT can therefore be used as an encoding for ANNs, where a CPPN computes the connection between each node in a network with fixed topology as a product of the pair on nodes queried. However, traditional ANNs do not have a specification of the relative positions of its nodes; it is a flat structure with no spatial properties. By giving the nodes in ANNs a relative position in space and use these coordinates as inputs to CPPNs, HyperNEAT is able to train ANNs with spatial awareness, and thus reflect a structure with more resemblance to biological brains where the relative position of neurons indeed plays an important role with regards to connectivity. Experiments in (Gauci and Stanley, 2010), reveals that if the geometry of the ANN is situated as the basic geometry of the problem (e.g. a checkers board), then HyperNEAT effectively use this geometrical knowledge about the problem to train ANNs that more easily handles geometrical relations and regularities.

Chapter 3

Implementation & Methodology

3.1 Getting familiar

We mentioned earlier that the EEG signal could be classified by the 3 Ns (noisy, non-linear and non-stationary), and that this could result in some issues when applying FFT to an EEG signal. An analysis of the effect of the violation of an assumed stationary (periodic) signal is the appropriate way to get familiar with what to expect from a classifier based on an EEG signal that has been transformed by FFT to the frequency domain.

Let us first of all introduce the dataset we will use to train and test our model. Koelstra et al. (2011) have made a database publicly available that consists of physiological signals (including EEG) and video recordings of 32 participants watching different music videos. The videos watched are a collection of 40 videos chosen among 120, because these 40 was found to induce the most emotions trough large scale screening. This screening was performed online, where participants rated movies on continuous scales for valance and arousal. Each movie was then segmented into 60 seconds time frames with a 55 seconds overlap, where the 40 segments that had the maximum emotional content was chosen. A relevance vector machine was trained on features such as colour variance, video rhythm, shadow proportions , and other similar features found to evoke emotions (see Koelstra et al. (2011) section 6.2 for a complete overview), to detect the maximum emotional content.

The participants were a population of 32 healthy individuals (50% female), with age between 19 and 37 (26.9 mean). Each participant was presented with a trial case, followed by a 2 minutes baseline recording without the experimenter, which allowed them to familiarize with the system before the actual recordings. After this,

the 40 trials was performed, and included the following steps: (1) informing the participant of their progress; (2) 5 seconds baseline recording; (3) displaying one of the 40 music video segments, and; (4) self-assessment of valance, arousal, dominance and liking. Self-reported data was gathered using the well establish method of self-assessment manikins (SAM)(Bradley and Lang, 1994), where arousal and valance was continuous scales with values from 1 to 9, and thus easily transferrable to Russell's circumplex model.

Considering their EEG setup, which had a sample rate of 512Hz over 32 electrodes with positions given by the 10-20 system, then the EEG part of the dataset consist of 32 participants each with 40 trails, where each trail consists of 33280 data points (2560 baseline and 30720 with video stimuli) for each of the 32 electrodes. This makes up a vast amount of raw data and is, by the authors, described as the largest publicly available dataset of affective data. A pre-processed edition of this dataset is however available. This is down-sampled to 128Hz, had its EoG artifacts removed, and was filtered to 4-45 Hz. The EEG signals is also averaged to the common reference, and a 3 seconds baseline was removed from data.

By choosing the 14 available electrodes in the Emotiv EPOC headset, from the list of 32 available electrodes according to the 10-20 system, then the final dataset we use includes 32 participants with 40 trials, where each trail has 14 electrodes with 8640 datapoints (384 baseline and 7860 with video stimuli respectively). The same self-reported levels of valence and arousal are accompanied both the raw and pre-processed dataset.

So with a clear picture of the formatting of the dataset, we can begin to investigate the actual signals. According to (Nunez and Srinivasan, 2006), the assumption of stationary (periodic) signal may be misleading; if we force the signal to be periodic by creating time frames and apply FFT on these time frames, then one does not have to care about how the signal behaves outside that interval, and thus to some extent forcing the signal to be periodic. This does however produce smearing into other frequencies, by the frequencies within the time frame that do not complete and integer number periods. To counter this, (Nunez and Srinivasan, 2006) displays the use of a windowing function (Hanning) that forces the signal towards zero at each end of the time frame, which removes the smearing from the aperiodic frequencies by artificially forcing them to be closer to periodic. The use of windowing functions has the effect of lowering the frequency resolution, and may therefore produce smearing in other frequencies, but as pointed out by (Nunez and Srinivasan, 2006), the use of a windowing is naturally more important as the total length of the time frames decreases. Figure 3.1 (a) and (b) displays the effect of a 128 definite time frame

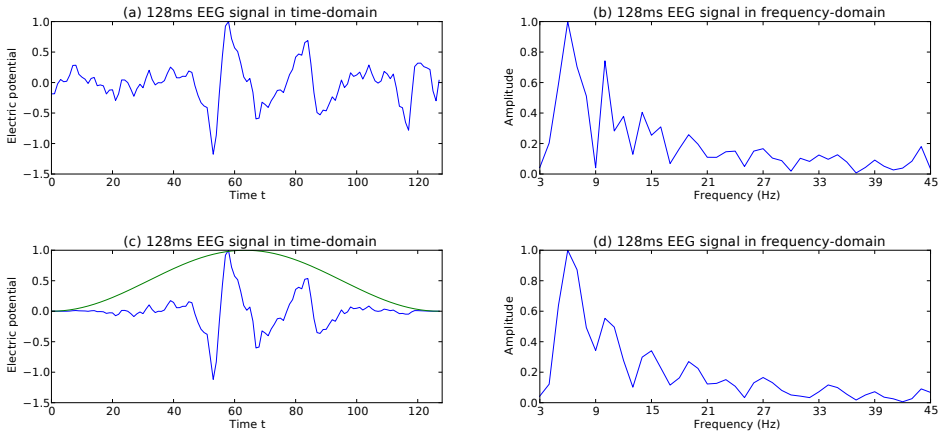

Figure 3.1: EEG signal before and after transformation. (a) Is the original signal from 128 datapoints, and (b) is the signal in frequency domain transformed with FFT. (c) Is the signal modulated with a window function (green) that forces the signal to be more periodic, and (d) is the modulated signal in the frequency domain transformed with FFT

that has been transformed from time domain to frequency domain without the use of a window function. Figure 3.1 (c) displays the same time frame in time domain multiplied by a window (green), and (d) displays the result of the transformation to this modulated window. It is clear from this lone example that the windowing function has an effect on the result. The most easily detectable changes are the increase in amplitude in 9Hz and 44Hz, and the decrease in amplitude in 13Hz and 25Hz, and the overall lower resolution compared to the transformed signal without a windowing function.

The previous example is very descriptive in in qualitative terms, but provides no quantitative measures of the effects of a windowing function. That is, it gives no direct indication of whether to use such a function or not. A more quantitative approach can be seen in figure 3.2. It displays the mean standard deviation for the amplitude of every whole frequency, for every 128 data point window, for every channel, for every trail and every participant in the reduced 14 channel dataset. It is here evident that the windowing functions works as expected; it does lower the variability of the dataset, by a good portion, by forcing the time frames to be periodic. Its effect is most noticeable in the 4-14Hz band, especially between 4-8Hz, but is quite noticeable among the whole spectrum with a lower mean standard deviation.

It is also evident in either case, that the standard deviation of frequencies from 4-14Hz has a greater variation than those from 14-45Hz, which is an interesting observation and points in a direction for what portion of the signal that is appropriate

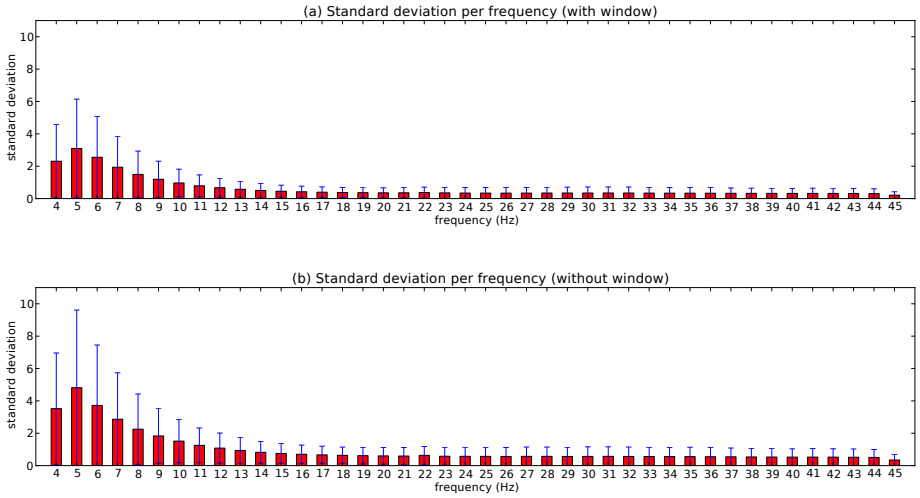

Figure 3.2: The mean standard deviation per frequency from each 128 datapoint time frame transformed by FFT, for each of the 14 available channels, for each of the 40 trails, for each of the 32 participants. (a) Is modulated with a windowing function (Hanning) before transformation, and (b) is transformed using only the raw signal.

to generalize over. We say point in a direction here, because a conclusive answer is hard to obtain, and the reason for this uncertainty is quite intricate. First, we have that each trial is classified by a single self-assessment, that is, one class per 60 seconds trail. Whether or not this is reasonable may be debated, but is never the less the appearance of the largest dataset on affective data available to date. A reasonable assumption is, however, that the rhythms of the brain do change during the duration of the video; it is indeed a dynamically shifting visual and auditory stimulus, and will most certainly produce variations among the recorded samples within a trail. We further saw that the frequencies in the range 4-14Hz was the frequencies with the highest variations in the 4-45Hz EEG band, which also means that they will be difficult to extract some sort of underlying rhythm from, that encodes for an emotional state. Nunez and Srinivasan (2006) does further complicate things by stating that as long as obvious artifacts are removed, then high amplitudes usually mean a high signal-to-noise ratio in EEG. As we have seen in previous examples, and in figure 3.3 which displays the mean amplitude for every participants (including each of the 14 channels and each of the 40 trails), it is clear that the highest amplitude waves is located in the first few frequencies, as expected (slow frequency, high amplitude). By using the statement by (Nunez and Srinivasan, 2006) directly, one may be lead to the conclusion that the lower frequencies naturally have a high signal-to-noise ratio; that may well be the case, but for completely other reasons. The statement should be interpreted as high amplitude compared to a default level

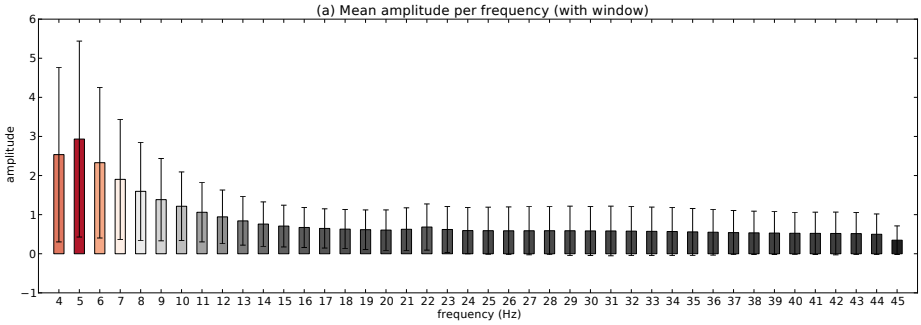

Figure 3.3: The mean amplitude for every frequency from each 128 datapoint time frame transformed by FFT (with window function), for each of the 14 available channels, for each of the 40 trails, for each of the 32 participants

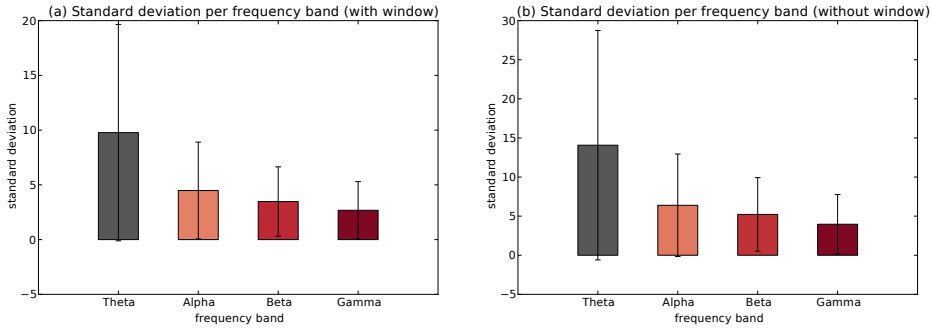

Figure 3.4: The mean standard deviation per frequency band from each 128 datapoint time frame transformed by FFT, for each of the 14 available channels, for each of the 40 trails, for each of the 32 participants. (a) is with the use of Hanning window, and (b) is withouty

of amplitude, which then makes perfect sense: whenever a frequency has higher amplitude than normally seen, then it is easier to distinguish from default noise and same-frequency artifacts. The total signal-to-noise ratio will thus not directly be lowered by excluding some frequency areas. A total loss of information is however inevitable, but may well be worth it in terms of accuracy in a model, if the remaining frequencies holds enough information to correctly identify the model's target phenomena.

By summing up the amplitudes in the typical EEG-bands, theta (4-8Hz), alpha (8-13), beta(13-30) and gamma (30+) (Koelstra et al., 2011), and measure the standard deviation with the same procedure as 3.2, as shown in 3.4, it becomes evident that if using these bands, then their order of inclusion is gamma, beta, alpha and theta, respectively. That is, finding the most descriptive combination of bands in terms of accuracy by starting with gamma and gradually including more bands in the order of minimized variation, and thus maximizing accuracy.

Another interesting observation is that the high frequency EEG bands which we have identified as the lowest in variation in the reduced dataset used, typically the beta band, has a change (increase) in activity when a subject is under the influence of benzodiazepines which is a drug commonly prescribed for general anxiety, panic attacks, insomnia and as a muscle relaxant, all of which could be related to temporal emotional states (Sanei and Chambers, 2008; Stern and Engel, 2005; Van Lier et al., 2004; Mohler et al., 2002). In fact, Van Lier et al. (2004) points to studies that find increasing beta and gamma activity when attention and arousal increases in subjects, even in drug free conditions. Even though being contradictory findings, a sedative drug and increased arousal do both increase activity, it does point in a tendency where the change in beta and gamma activity reflects the change in behaviour of the subjects through modulated intensity of arousal and attention. While this supports the high frequency bands as being informative, Nunez and Srinivasan (2006) states that even though these bands are included as important for general brain function, their low amplitude makes them harder to distinguish from artifacts than bands that typically has higher amplitude.

3.2 Implementation

We decided to implement HyperNEAT ourselves in the Python programming language, with the Python implementation of NEAT, as published on Stanley's NEAT user page[1], as the basic underlying NEAT module. The reasons for not using one of the implementations from the HyperNEAT users page[2] are in our case many. Quite subjectively, we prefer to use Python as it combines expressiveness from multi-paradigms, dynamic typing, and a clear syntax with a reasonable performance. It is also easily compatible with Matlab and C++. More objectively, emokit, the only open-source project developed to enable gathering of raw data from the Emotiv EPOC headset without the use of the expensive software from Emotiv, is written in Python. Our implementation could therefore directly be integrated in emokit in the future, without the need for any tedious cross-language imports or compilations.

3.2.1 From NEAT to NEAT-CPPN

NEAT are able to effectively evolve CPPNs by gradual complexification, like mentioned earlier. The transition of going from a NEAT system that evolves ANNs, to

[1]NEAT users page: http://www.cs.ucf.edu/~kstanley/neat.html
[2]HyperNEAT users page: http://eplex.cs.ucf.edu/hyperNEATpage/HyperNEAT.html

a NEAT system that evolves CPPNs is quite simply to allow for a diverse repertoire of activation functions in the evolved networks, where the choice of which activation function to use in a newly introduced node (gene) is random. So any new node introduced by gradual complexification (mutation) is assigned a random activation function, from a set of available functions that typically are symmetrical, periodic, or linear. Gauci and Stanley (2010, 2011) did in their checkers and scalable go experiments use Sine, Gaussian, sigmoid and linear functions. The same set appears in Woolley and Stanley (2011) which evolves a robot arm controller. Stanley et al. (2009) used a combination of sigmoid, Gaussian, absolute value, sine and linear. This list, with small variations, appears as a solid foundation for a set of activation functions. Our set of activation functions is then as follows:

Table 3.1: Set of activation functions

Name	Function
Gaussian	e^{-x^2}
Tanh	$\tanh x$
Sine	$\sin x$
Linear	$\frac{min(max(x,-3.0),3.0)}{3.0}$
Bool	if $x > 0$ then 1 else 0

where the Gaussian and Linear functions are a direct implementation from the source used in (Gauci and Stanley, 2010). This means that for any new node added through mutation, a random choice decides which of these functions that will serve as the activation function for that particular node trough the lifetime of that gene (constant as long as the node is still included in an individual in the population). We also decided to use signed activation with a range from -1.0 to 1.0, to ensure a predictable output range from the CPPNs. The tanh function serves well for this task, and is thus our choice for output nodes.

To summarize, CPPNs evolved by our system can then have an arbitrary number of inputs, with an arbitrary number hidden nodes with different activation functions, and an arbitrary number of output nodes with the hyperbolic tangent as activation function. The number of input and output nodes is naturally given by the nature of the problem one is investigating. Take for instance an intensity map restricted by N x M values. If a CPPN was to be evolved to approximate its underlying function, then a typical setup for the CPPN could be two input nodes which take the coordinates of the two different dimensions as input. A normalized range from -1.0 to 1.0 is preferable here since it facilitates the evolvement symmetry and periodic behaviour from the network. The output node could then simply be a single node

with an unsigned activation function that outputs the intensity at point x y in the range from 0.0 to 1.0.

3.2.2 Using NEAT-CPPN to evolve Substrates

Algorithm 1 HyperNEAT algorithm (Adapted from Gauci and Stanley, 2010)

Input: Substrate Configuration

Output: Solution CPPN

Initialize population of minimal CPPNs with random weights

```
1:  while Stoppingcritaria is no met do
2:      for each CPPN in the population do
3:          for each Possible connection in the substrate do
4:              Query the CPPN for weight w of connection
5:              if Abs(w) > Threshold then
6:                  Create connection with weight scaled proportionally to w
7:              end if
8:          end for
9:          Run the substrate as an ANN in the task domain to ascertain fitness
10:     end for
11:     Reproduce CPPNs according to NEAT
12: end while
```

This part of the implementation consists of using CPPNs evolved by NEAT to encode for the connection topology of a substrate (ANN) and is the heart of the HyperNEAT methodology. We will here explain our implementation by a stepwise referral to the basic HyperNEAT algorithm as presented in Algorithm 1.

Starting with the substrate configuration, which is the input in Algorithm 1, we decided to separate the geometrical and actual configuration of the substrate. This means that we store all the coordinate pairs for all available connections in a substrate separate from the definition of the network in terms of activation functions, actual connections, and nodes. The reason for doing this is strictly due to performance and allows us to make a pre-defined list of inputs to the CPPNs, as inputs to the CPPNs are not necessarily restricted to the coordinates of the problem. Such additional inputs, along with the coordinates, may be the coordinates distance from centrum, their relative distance from each other, as well as other primitive helper functions to the CPPNs. Stanley (2006, 2007) uses distance to the centre as an

extra parameter when evolving symmetric and periodic patterns with good results. He explains the gain of giving the CPPN a value that it could easily approximate by itself (distance from centre), by pointing out that functions higher in a gradually evolved CPPN have a direct reference to the absolute distance at any time, even though their inputs may be periodic. It is a helper function in other words. The separation does therefore allow us to restrict the computational overhead of such a helper function by only performing it only once in the beginning of each run.

Line 1 and 2 in Algorithm 1 is naturally given by the problem one are to investigate, but a stopping criteria is typically a threshold in number of generations and evaluations, or an appropriate threshold in fitness. Line 3 is related to the previous mentioned separation of substrate configuration, where the enumerable list of possible connections is in our implementation substituted with the pre-calculated list of coordinates of the endpoints for every possible connection, along with the possible helper estimates.

We implemented line 5 and 6 according to (Gauci and Stanley, 2010), which means that any connection whose weight, as outputted by the CPPN, with absolute value is above 0.2, results in a connection in the substrate scaled proportionally to a range of 0 to 3, and that any connection with a weight less than this threshold results in a weight of 0.0. This effectively allow HyperNEAT to disable connections if found beneficial. A formal definition of this operation is shown in equation 3.1.

$$w_{scaled} = \begin{cases} scale(w) & \text{if } 0.2 < |w|, \\ 0 & \text{if } 0.2 > w > -0.2\ . \end{cases} \tag{3.1}$$

Line 9 is naturally given by the specific problem, and our implementation allows for any types of functions or modules to be used here. Line 10 is given by the implementation of NEAT-python, and follows the implementation in (Stanley and Miikkulainen, 2002b) with the modifications needed to implement the NEAT-CPPN according to (Stanley, 2007) and as described in the previous section.

3.2.3 Optimization

Tournament selection is, when used in evolutionary systems, a local selection mechanism which is highly controllable in terms of selection pressure. Selection pressure is intuitively referring to the likelihood that a given individual, with a given fitness, is chosen for reproduction. That is, if the pressure is high, then mostly the fit individuals (highest fitness according to the fitness function) will be selected for

reproduction. If the pressure is low, then those individuals with mediocre or poor fitness have a higher probability of reproducing. Heritability and diversity—how genes are passed on, and the total available gene pool within the population—is therefore naturally affected by the selection mechanism. By definition, tournament selection is controlling the selection pressure with two available parameters: k and p, where k is the tournament size in terms of numbers of individuals drawn at random from the population, and p is the probability that the individual with the highest fitness in the tournament is selected. Knowing this, it is easy to see that if both k and p are at their lowest functional value (e.g. $k = 1$ and $p = 0$), the selection of parent(s) for reproduction is done at random, and is therefore projecting the underlying fitness distribution of the population in question. A high value of k and p (e.g. $k = N$ and $p = 1$) will then project only the best fit individual(s).

NEAT-Python, which is our underlying NEAT module, implements tournament selection as the primary selection mechanism, or at least partially implements it. The population is first sorted by fitness before performing truncation (removal of a fraction of the total individuals which are considered too poor performers) and elitism (copying of the best individual(s) from the current generation to the next, to ensure that a good solution is not lost in the reproduction process). The entire population within a species is then randomly shuffled, and the best fit individual of the first k individuals is the chosen for reproduction. Considering the entire population N of different species, this has to be done at least $2 \times N$ times to avoid a reduction of N, as each couple of parents produce one offspring. Two key aspects of tournament selection are lost by this implementation: (a) the controlling of selection pressure, simply because $p = 1$ and k is hardcoded to two; (b) the natural lightness in computational complexity that tournament selection holds, because it requires no sorting of the population. In defence of the authors of NEAT-Python, we must include that it is a work in progress and should be treated thereafter. However, we feel that it was necessary to re-implement tournament selection, and make the parameters easily available when testing. This new implementation allow for the adjustment of both p and k through the config file, as well as replacing the shuffling of the entire population within a specie, by instead randomly picking individuals from the same population k times.

3.3 Exploration of geometrical generalization

Implementing a pre-defined methodology like HyperNeat, partly from scratch, instead of using an open source distribution does both have its advantages and disadvantages. The obvious disadvantages are mainly that fewer persons get to look at the actual code, and even fewer get to run independent experiments with the finished implementation. We are in effect the only quality control for ourselves, and before defining our model formally in next section, we would like to present an exploratory test which is designed to highlight the implementations abilities to produce ANNs that are trained by the geometry of a problem. Keep in mind that this is only exploratory test, and not meant as a statistical proof of concept.

In the spirit of the checkers experiment in (Gauci and Stanley, 2010), we decided to test our implementation by a 4×4 connect four game versus an existing computer component. Unlike checkers with its 5×10^{20} possible positions, our 4×4 grid connect four has 161029, so it is quite less complex. Never the less, both are geometric in nature, and both are strongly solved (checkers by Schaeffer et al. (2007) and connect four by John Tromp[3] (1995))

The choice of a 4×4 grid is not arbitrary, where the reason for choosing these numbers stem from the basic geometry of the EEG-specifications in our setup. The basic electrode count in Emotiv EPOC is 14, and these exact electrodes are the one we use in our reduced dataset for later testing. A 4×4 grid is then just above the complexity of our EEG-data in terms of geometrical positions, and might therefore tell us something about the implementations capabilities to generalize over this scale of geometrical inputs.

A worthy opponent is found in Al Sweigart's connect four game[4], which is a python implementation of connect four that allows a human player to play against a computer opponent. The computer opponent is making its decisions based on a depth first search in a n-ply game three, where each move is assigned 1, -1 and 0, coding for win, loss and neither. From the returned list of potential moves, the move with the highest returned value is chosen as candidate. However, if the list of potential moves got more than one candidate with the same value, then a random choice between the moves decides the final candidate. Two interesting aspects can be seen here: (a) the computer does return 0 for any other moves that does not directly lead to a winning or losing position, and; (b) the computer player is non-deterministic. The first aspect (a) is clearly exploitable by an evolutionary system,

[3]Connect four db: http://archive.ics.uci.edu/ml/datasets/Connect-4

[4]Connect four game: http://inventwithpython.com/fourinarow.py

but (b) makes it troublesome to assess the fitness of an individual in the population, which clearly leads to distortions in the search space.

The HyperNEAT evolved substrates that will be the opponents to Al's AI, follows the three layered configuration in (Gauci and Stanley, 2010). This means that the input layer is 4×4 nodes, where each node is situated at the available board fields, and that the hidden layer has the exact same appearance as the input layer. The output layer is simply just one node that outputs an estimate of the desirability of any given board state. Both the hidden layer and the output layer uses tanh as activation function, so the output from the network is restricted between -1.0 and 1.0. Board states are inputted to the network by letting every empty space have the value of 0, and spaces occupied by red and black pieces have the value of 1 and -1 respectively.

We had to restrict the n-ply search of the game tree to 3 moves look-ahaed, since the original experiment does not implement any pruning which leads to an exponential growth of the trees, and therefore also an exponential growth in execution time. We could have implemented the pruning ourselves, to allow for faster execution and possibly deeper game-trees, but that would essentially ruin the idea of rapidly testing our implementation versus a pre-defined opponent. More important is that the goal with this test is not to evolve a *perfect* connect four player, but instead see the implementation's ability to generalize over geometry in order to produce a *good* player versus the opponent given. To make it even more interesting, did we not allow the evolved substrates to look ahead in a game tree, and thereby forcing more long term tactics. This is unlike the substrates evolved in (Gauci and Stanley, 2010) where both the substrate and the opponent was allowed to assess every board state in a 4-ply game tree.

Every individual in the HyperNEAT population had their fitness determined by playing complete games versus the existing AI, where a win was given 1 in fitness, a tie was given 0.5 and a loss resulted in 0. The results were averaged over ten runs in order to better cope with the non-determinism in the opponent. Parameters used in this test can be found in appappendix 1 which is a combination of previously used parameters for NEAT (Stanley, 2007) and HyperNEAT (Gauci and Stanley, 2010), found to be robust for many experiments, and parameters found to perform well in preliminary tests.

Running a population of 100 individuals through 100 generations revealed a solution with 0.9 in fitness according to the fitness function, as the best individual. Allowing this solution to play against the existing AI for 100 complete runs

resulted in 63 wins, 31 defeats and 6 draws. This is quite impressive against a non-deterministic 3 move look-ahead opponent.

One important finding in (Gauci and Stanley, 2010) is that general players performed better than specialized players in checkers, and that the general CPPNs had a smooth connectivity patterns, while the less general players had a discontinuous and jagged connectivity pattern. Figure 3.5(a) and 3.5(b) shows the connectivity patterns produced by the winning individual in our 4×4 connect four problem, where (a) is the connectivity pattern between the input layer and the output layer and (b) is the connectivity pattern between the hidden layer and the output layer. Both of these patterns are smooth and continuous, so the winning individual is indeed a general connect four player. Closer examination of the figures reveals that the tactics involve a desirability of controlling the game from left to right from the connectivity pattern between the hidden layer and the output layer, and a desirability of controlling the rows from the bottom up in prioritized order between the input layer and hidden layer.

Such connectivity patterns give unique insight in solutions evolved by HyperNEAT. The connectivity patterns produced by an individual give *meaningful* explanations of the behaviour of the substrate. This is possible because the networks are trained by the basic geometry of the problem, and the layers of the networks are configured to be situated at this geometry, which reveals the attractiveness of positions and specially the attractiveness of a position with regards to how the opponent is positioned.

Figure 3.6–3.8 shows different game states from a single run that is very descriptive in how the overall strategy, as seen from the connectivity patterns, results in a good connect four player for our particular setup. The top row of the figures (a)–(c) stems from the evaluation of the game state before performing a move, where: (a) is the receptive field of the hidden layer (how the hidden layer *sees* its inputs); (b) is the receptive field of the output layer; (c) is the activation levels of the hidden layer. The second row (d)–(F) displays the same types of patterns as the above row, where the difference is that these patterns stems from the evaluation of the board state that led to the actual move. The last row displays the pre-move board state (g), and the post-move board state (h).

Figure 3.6 shows the response to the first enemy move. The substrate performs a counter move in vertical direction, which is the result of the maximization from the evaluations of the four allowed moves from the pre-move board state. A comparison of the two first rows reveals the explanation for this move. The receptive fields

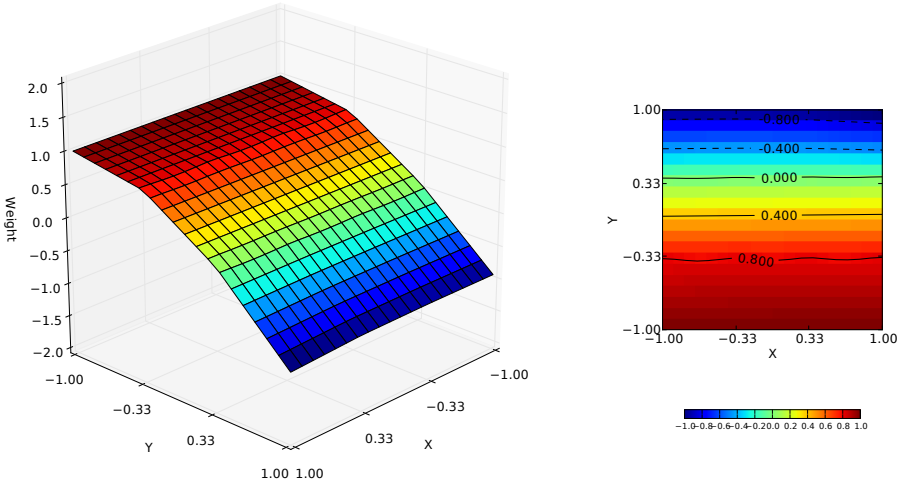

(a) Evolved connective pattern (Input-to-Hidden)

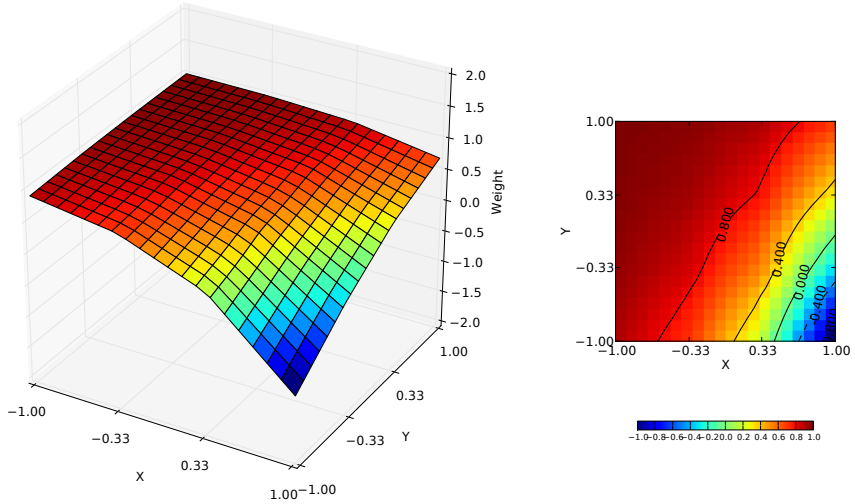

(b) Evolved connective pattern (Hidden-to-Output)

Figure 3.5: The connective patterns produced by the winning individual in the 4×4 experiment, visualized as planes and topographic maps, where (a) is the connective pattern between the input layer and the hidden layer, and (b) is the connective pattern between the hidden layer and the output layer.

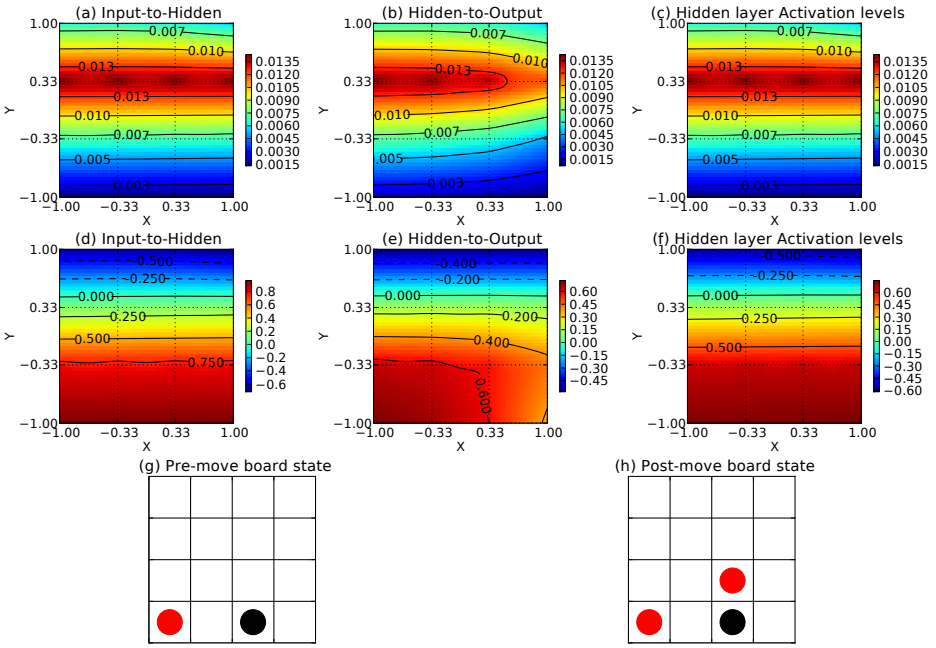

Figure 3.6: The counter move for the first enemy move (black). Figure (a) and (b) is how the substrate sees the board state after the enemy move, represented as a recetive field for the hidden layer. Figure (c) shows the hidden layer activation layer. The second row displays the same as the above row, but is instead the receptive fields and activation levels for the winning counter move. The pre and post move board states are shown in (g) and (h) respectively

in (a) and (b) yields a low overall input both to the hidden layer and the output layer, particularly in the lower area of the board. This is reflected in a low level of activation from the hidden layer (c), and a low overall score of the board state, which is quite natural because the evaluation is performed just after the enemy's initiative. The receptive fields in (d) and (e), resulting from the maximum evaluation value, yields a much higher input to both the hidden layer and the output layer and therefore a much higher activation of the hidden layer, and a high evaluation of the board state from the output layer. We can see here that this particular counter move leads to receptive fields that is true to the underlying tactics, where (d) has the resemblance of the connectivity pattern produced by the CPPN between the input layer and the output layer, and (e) is a combination of both.

Figure 3.7 shows the evaluation of a mid-game board state. The evaluation of the pre-move board state does also here lead to low inputs to the hidden layer and output layer as seen in (a) and (b). An interesting behaviour is seen when looking at the move given by the maximum evaluation of legal moves. Even though being outside most positive influential area from the connectivity pattern between

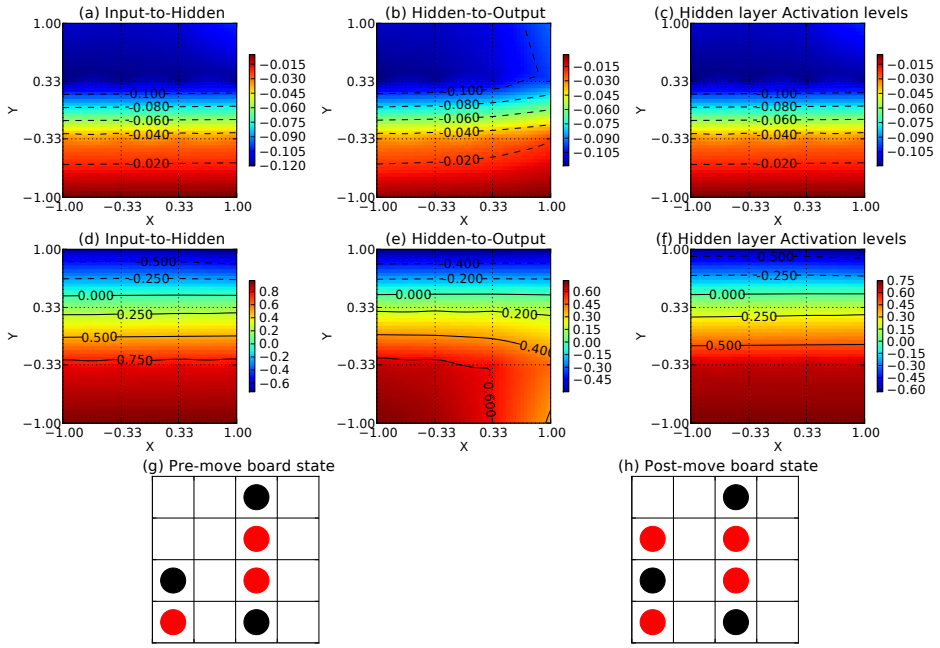

Figure 3.7: A mid game board state can be seen here. Notice that the two stacked pieces in cloumn 3 shows that the substrate took initiative in the previous move. The figure follows the same layout as in 3.6

the input layer and hidden layer, it is still the move that results in a pattern with the most resemblance to the original connectivity patterns and thus the original strategy, as seen in (d) and (e). The behaviour prioritizes to counter enemy threats by placing a piece directly on top of the enemy piece, instead of stacking from the bottom up regardless of the opponents moves.

The winning move can be seen in figure 3.8. While the move itself is not very interesting (it is indeed the only legal move), it does nevertheless show that the winning move does also show a great resemblance to the original connectivity patterns and therefore the original strategy. A closer look on the board states reveals that an enemy move occurred at some point that posed little threat to the strategy, with the stacking of red pieces as a result (column 3 in (h)). The behaviour of the substrate is therefore passive-aggressive, and does only take initiative when beneficial.

This exploration of our implementation by the use of a geometrical problem that is slightly more complexity in terms of inputs, displays that our implementation is indeed capable of generalizing over the geometry of such a problem. The winning CPPN from the Connect 4 problem encoded for a substrate with a passive-aggressive behaviour with regards to the geometry and the opponent. It stacked pieces in columns above enemy pieces when appropriate, and above own pieces when beneficial. The stacking in height in separate columns is the result of the long-term

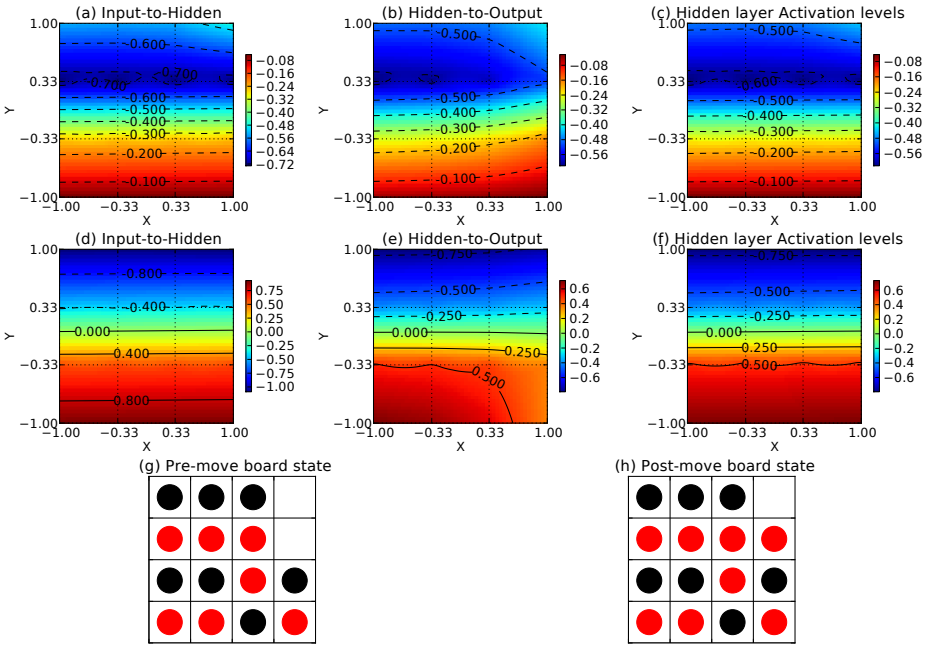

Figure 3.8: The winning move can be seen in this figure. The substrate has correctly avoided the 3 move look ahead of the oppnent, and managed to place the pieces in such way that a win is certain.

strategy needed to defeat the 3 move look-ahead opponent, exploiting the fact that there is no assessment of intermediate states (the opponent sees any other board states than states that directly lead to a win or loss as equal). By the time the opponent sees the threat it is usually too late, where any combination of moves leads to a victory to the substrate evolved by the winning CPPN.

3.4 The model

We have in the previous sections seen a familiarization with the nature of EEG-signals, and examined what to expect when transforming the signal to the frequency domain by the use of FFT. We have also described our implementation of HyperNEAT and tested it on a problem with similar complexity in terms of number of inputs, with promising results. This section will formally define how the EEG-signal is presented to the substrate, and the configuration of the substrate itself.

3.4.1 Pre-processing

In the investigation of the EEG-signals we found several clues on how to get the most stable cases to generalize over by looking at what part of the signal in frequencies

that is the least variable, and how to reduce the variability of the dataset as a whole by forcing the signal to be periodic with a windowing function. This turns out to be crucial observations because the dataset only contains one self-assessment (class) per trail (example), which we want to use as ground truth for the assumed underlying waveforms encoding for the emotional states of the subjects.

The training examples is created by using averaging of the signal to uncover the underlying waveforms of the different subjects and trails, which is proven to perform reasonably well in other studies with lower electrode resolution than our EEG setup (Grierson, 2011). Even though it might sounds strange to apply averaging to a dataset gathered by showing continuously changing videos, one must assume that near identical emotions are felt within a trail, and thus making the changes in the waveform, caused by the the video and audio stimuli, just a varying and unwanted part of the signal.

More formally, the averaging technique consists of first segmenting the signal from a trail into equal length time frames, where the length of the time frame determine the statistical power of the result of the averaging of all time frames. The number of data points in the time frame does also determine the resolution of the frequency coefficients resulting from a FFT of a time frame. This indicates that there is a balance between statistical power of averaging, and the resolution of the frequency coefficients, where a more data points in a time frame gives a higher resolution in frequency coefficients, but lowers the statistical power of the averaging by restricting the number of time frames within a single trail. We naturally seek as high statistical power as practical with regards the resolution.

Let us first explain what this statistical power is in the context of averaging time frames from an EEG signal that have been transformed by FFT. The result X from a FFT of an N data point time frame is N/2 frequency coefficients with both a real part and an imaginary part (or complex conjugates for real valued FFT). The amplitude spectrum is obtained by taking the absolute value of X, and the power spectrum is obtained by squaring the amplitude spectrum like mentioned in Chapter 2.2. A power spectrum is thus an estimate of the power (and variance) of the signal as a function of frequency (Nunez and Srinivasan, 2006). An estimation of the power spectrum of the underlying stochastic process encoding for the emotional state of a subject is then obtained by averaging K number of time frames from the original trail, where an increase in K yields a more correct result (more statistical power).

It is also clear from the explanation above why the resolution is affected by the length of the time frames. A further restriction of the length is posed by the Cooley-

Tukey FFT algorithm which works most efficient for any power of two. So we have three restrictions: (1) maximization of K by a low N; (2) high enough N to at least have whole separable frequencies, up to the maximum frequency; (3) N has to be a power of two.

Solving for all reveals that when N = 128, then K is 60 (60 seconds trails, with 128Hz sampling rate), and every frequency in X is outputted as whole frequencies, in the most efficient way according to the specifications of the Cooley-Tukey algorithm. If we then apply the window function (as found to reduce the variance) before the FFT of each individual time frame, then it is evident that we use Welch's method (Welch, 1967) with zero overlap to get an estimate of the spectral density. The trails in the dataset can therefore be reduced to a set of frequencies and their respective power estimates. However, we want to look at the overall band activity from the typical EEG bands as presented in section 3.1, which allow us to further reduce the complexity of the problem by assuming that the total activation of the bands is sufficient to describe the underlying process. This assumption is naturally causing a reduction in resolution, but it do allow us to see the data from a more generalized perspective, which refers the Chapter 2 and our dissection of what these bands are, and that combinations of these bands are found to encode for cognitive states, behaviour, location on the brain, and so forth. The trails are therefore reduced to a set of the four EEG bands available from the frequency range from the dataset.

We feel that is appropriate to mention that treating the bands as complete entities is debated such as in (Nunez and Srinivasan, 2006) where an argument is proposed to show that one cannot safely treat the alpha band as a unitary phenomenon. This argument stating that different combinations of high and low (Hz) activity in the alpha band encodes for different cognitive processes are reasonable and may well be the ground truth. However, to our best knowledge, the use of a neuroevolutionary methodology in the task of generalizing over multi-channel EEG geometry has never been attempted before. Being first entails that the resolution *needed* to get the results *wanted* is unknown, where a natural starting point would be a method with relatively low resolution when choosing from the range of proven existing methods and gradually use more sophisticated methods if they improve the results.

To summarize, the pre-processing involves: (1) segmentation of the trails into 128 data point epochs; (2) Welch's method with zero overlap to estimate the power spectrum of the four bands (theta, alpha, beta and gamma).

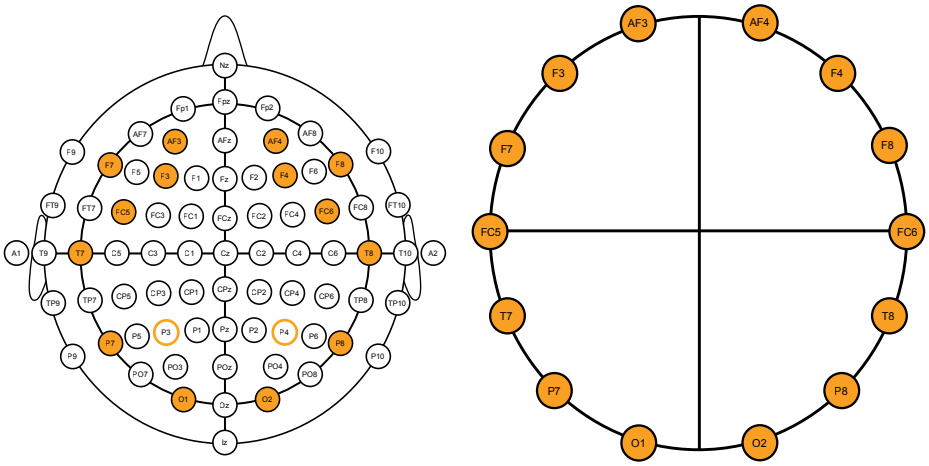

(a) The basic geometry of the Emotiv EPOC headset

(b) The adapted basic beometry

Figure 3.9: These two figures shows how the basic geometry of the Emotiv EPOC headset (a), as seen in two dimensions, is adapted for the basic geometry of the substrate's input and hidden layer (b).

3.4.2 Inputs

From the investigation of the signal, we have that the variance in the theta and alpha bands are higher (especially theta), than the variance in the beta and gamma bands, which leads to a higher degree of uncertainty in the estimated power spectrum from the theta and alpha bands. We also found interesting connections between emotions and the beta and gamma bands. Koelstra et al. (2011) has also found beta and gamma bands to have the highest number of electrodes in EEG to significantly correlate with emotions. Based on these findings, the final inputs to the system will be the estimated mean power of the beta and gamma bands for each trail, for each electrode in the 14 channel setup.

3.4.3 Substrate configuration

The substrate configuration in terms of geometry is by convention situated at the basic geometry of the problem in HyperNEAT. This means that our substrate will have layers that resemble the geometry of the EEG setup. Figure 3.9(a) shows in two dimensions the position of the electrodes in our EEG setup, while 3.9(b) displays how we adapt this geometry in HyperNEAT. The difference in electrodes AF3, F3, FC5, and their matching even numbered electrodes, is done to easily allow CPPN to exploit symmetry, asymmetry and periodic patterns in the input. The

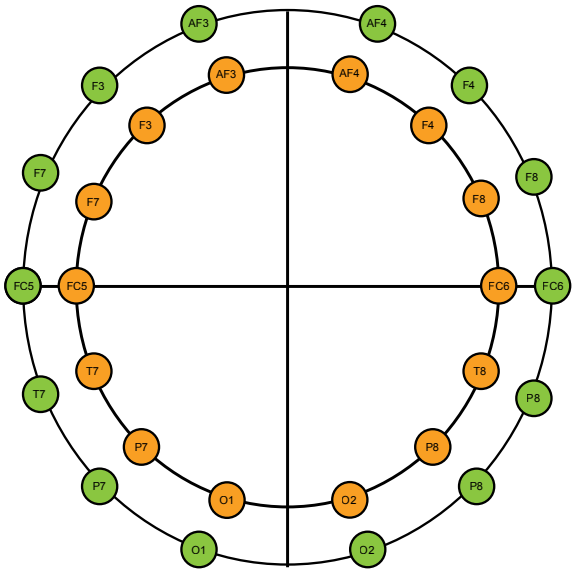

Figure 3.10: The adapted basic geometry, with the extension of two bands. The orange nodes are the beta band, and the green nodes are the gamma band. Both of these halos are defined by the same X and Y coordinates, where a parameter R, the distance from center, is the only indirect difference.

basic geometry of the substrate is therefore a halo in two dimensions with the 14 input nodes evenly distributed at each semicircle, where each position is given by Cartesian coordinates.

Figure 3.10 shows how we incorporate the two bands (beta and gamma) that stem from the same position when recorded. Instead of changing the Cartesian coordinates directly for the outer band, which is interpreted as at different positions by the CPPN, we included another dimension which is the radius R from the centre. The two bands do therefore have the same X and Y coordinates, but is indirectly different when R is supplemented to the CPPN. The CPPN can then decide if and when the separation of the two bands is beneficial, instead of starting with two different positions and approximating their similarity by polar coordinates.

Both the input layer and the output layer share the previously described basic layout, while the output layer is simply two nodes situated at equal but opposite positions, encoding for the outputs in the continuous two-dimensional model of emotions, as presented by Russell (1980), and used in the testing dataset recorded by Koelstra et al. (2011). The three layers are separated by their own dimension H, where -1 is the input layer, 0 is the hidden layer and 1 is the output layer. This is also done to allow the CPPN to easily distinguish between them, and use this information if needed.

From the defined layout, we now have that each CPPN must allow for 8 inputs,

which is the X and Y coordinate of an endpoint, along with R to separate the two bands and H which encodes for the layer the endpoint is member of. This makes 8 inputs for the two endpoints in a connection. The last piece of information given to the CPPNs is the relative distance between two endpoints of a connection, which makes sure that the CPPNs always have easy access to this value in higher functions (nodes), as discussed in section 3.2.2. So the total inputs to the CPPNs is 9, which means that the CPPNs draws the connective patterns for 2×4 dimensional hypercubes (excluding the helper function).

Chapter 4

Experimental Results & Discussion

This chapter will investigate the performance of the model from a quantitative perspective, supplemented by a qualitative dissection of one of the evolved individuals, in order to build a meaningful and reasonable answer to our research question as posed in Chapter 1.

4.1 The Experiment

The problem posed to the substrate is the task of detecting two different emotions from the subjects in the reduced test set, as presented in Chapter 3, and then output the correct values for each emotion in the two-dimensional scales of emotions that we and the dataset rely on. The two distinct emotions from each subject are chosen from the subject's list of self-assessments for all of the 40 trails with the basis of the sum of the values from the two dimensions, where the highest and lowest sum is chosen. This means that the two trails chosen from each subject is the highest and lowest scoring trails, as a combination of the two dimensions, based on the subject's own rating. An argument stating that two cases chosen on the basis of extremes are more easily distinguishable from one another than two cases with more similar ratings, is of course reasonable (but speculative). However, we are *not* testing to find out how the model perform on very similar cases, but instead true to our research question and therefore exploring if this methodology is a viable technique in our problem area. Choosing the extremes in terms of rating is then just an appropriate and objective selection protocol which allows us to compare the results from different participants, using the self-assessment of the participants as the ground truth.

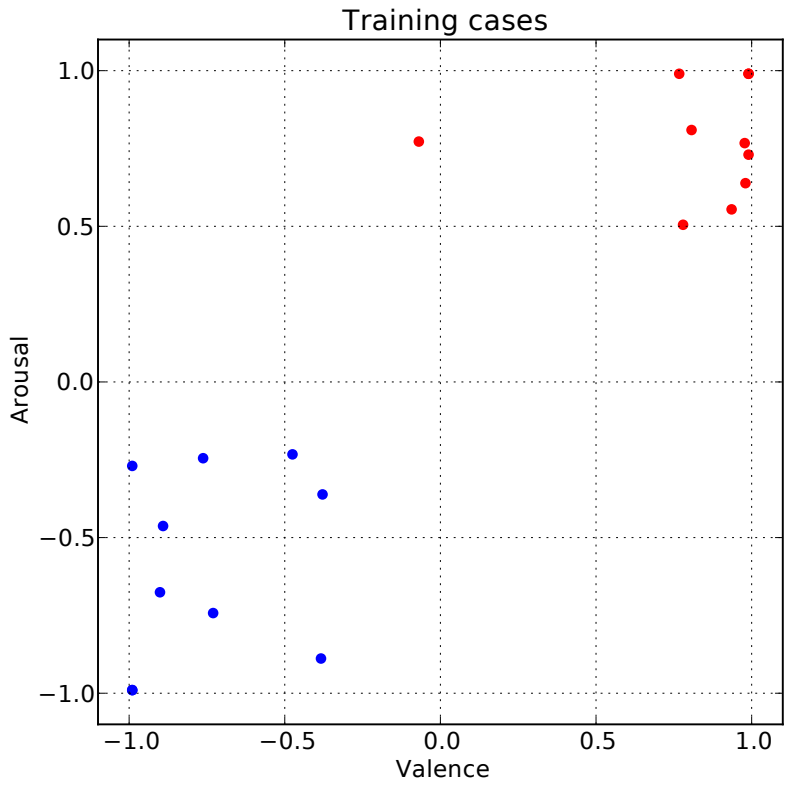

Figure 4.1: The training cases represented as points in the two dimensions of emotions. Red points indicates that this is the maximum rating of a pair of max/min ratings, while blue is the minimum.

Figure 4.1 shows the distribution of ratings from all the selected trails from the subjects, where red indicates that the rating is a maximum of a pair, and blue indicates a minimum (note that some are overlaying as the result of similar ratings). One interesting case can be seen here, where the maximum (red) rated trail is actually negative in valence. Table 4.1 displays each participant's maximum and minimum rating in trail numbers, as well as the actual rating for both of these trails. The ratings are in the dataset reported in a range from 1 to 9, but we have scaled them proportionally to a range of -1 to 1 to later facilitate the use of tanh as activation function in the output layer of the substrate.

The substrate configuration used in this experiment is the configuration deducted in Chapter 3, which means that the input layer and hidden layer of the substrate has a circular geometry where each electrode position is given in Cartesian coordinates. The circular geometry is two halos, one for each band included in the test cases, where the 14 electrodes are evenly distributed in their respective pairs on each semicircle, on both halos. The X and Y coordinates of the electrodes is identical on

Table 4.1: Selected trails from each participant

Sub. num.	Trails	Max	Min
01	[20, 28]	[0.99, 0.73013]	[-0.9009, -0.67568]
02	[2, 20]	[0.99, 0.99]	[-0.99, -0.99]
03	[33, 24]	[-0.0693, 0.7722]	[-0.38362, -0.88853]
04	[2, 36]	[0.97762, 0.76725]	[-0.99, -0.99]
05	[1, 37]	[0.99, 0.99]	[-0.99 , -0.26977]
06	[6, 22]	[0.80685, 0.80932]	[-0.37867, -0.36135]
07	[35, 27]	[0.76725, 0.99]	[-0.73013, -0.7425]
08	[8, 29]	[0.93555, 0.5544]	[-0.891, -0.46283]
09	[12, 32]	[0.77963, 0.5049]	[-0.4752, -0.23265]
10	[6, 24]	[0.9801, 0.63855]	[-0.7623, -0.24503]

both halos, where a distance R is the only separation of the two bands. This allows us to indirectly inform the CPPNs that there is a distinct difference between the two points without explicitly giving the CPPNs separate coordinates. In fact, to explicitly give different coordinates for the same electrode for the different two bands to the CPPNs would not be in line with the basic geometry of the problem area, which is a direct violation of the HyperNEAT methodology, since both the bands stem from the same electrode and therefore also the same geometrical position. The output layer is simply two nodes; one for the arousal scale and one for the valence scale. Both the hidden layer and the output layers in the substrate uses tanh as activation fuction. An overall figure of the substrate, as well as a visualization of parameter H can be seen in Figure 4.2(a). Parameter R is visualized in Figure 4.2(b), along with the basic geometry of the substrate.

The CPPNs used in this test is also configured as described in Chapter 3, where the 9 inputs is the pair of X and Y coordinates from the endpoints of a connection in the substrate along with the separation parameter R, the layer indicator H, and the distance between the two endpoints. The outputs from the CPPNs is separated by two output nodes, where one is used to create the connective pattern between the input layer and the hidden layer of the substrate, and the other is used to create the connective pattern between the hidden layer and the output layer. We chose to allow the CPPNs to be fully connected from initialization, that is, allow the input layer to be fully connected to the output layer. This design choice might sound counterintuitive with regards to NEAT's philosophy of starting from a minimally complex topology, but by allowing the CPPNs to be fully connected from start we do ensure that there is no bias towards any particular input after the initialization,

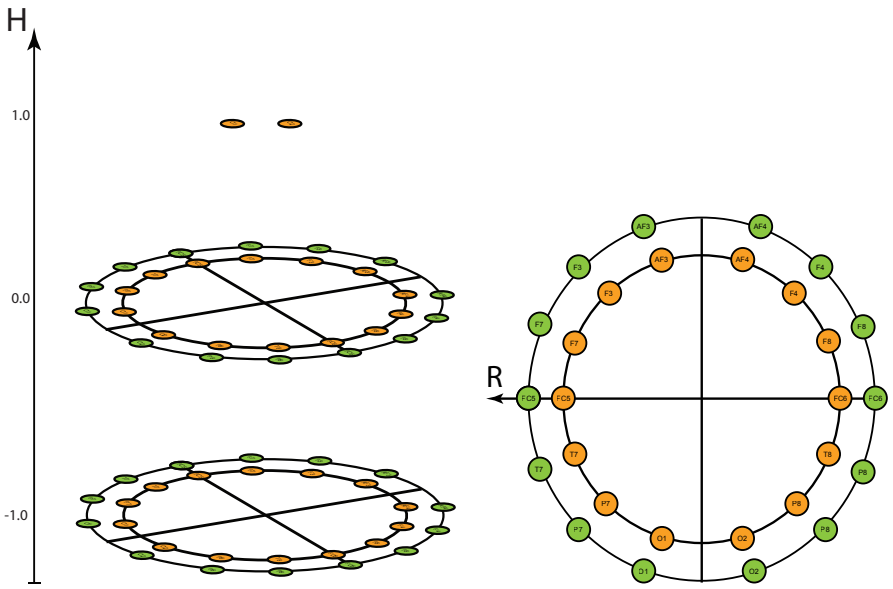

(a) Parameter H (b) Parameter R

Figure 4.2: (a) shows the parameter H as well as the overall structure of the substrate used, and (b) shows the parameter R as well as the adapted basic geometry, including both bands, as used in the input and hidden layer.

which makes perfect sense with regards to the HyperNEAT philosophy of generalizing over the overall geometry of the problem, and not only parts of it. NEAT is of course able to disable the link from any input at any time through mutations (disable link mutation), if found beneficial, but this is again the result of evolution, where evolution has *found* that the most correct behaviour is achieved by excluding some of the inputs.

The parameters used in this test are listed in appendix A, and is the combination of parameters found in the literature to be robust on a range of different problems, with minor adjustments found to give a more gradual increase in fitness, compared to a stepwise increase which often indicate that the system is based on lucky mutations. The most noticeable adjustment is the adjustment to the weight mutation power. In the checkers experiment in Gauci and Stanley (2010), they used a weight mutation power of 2.5 whereas we found 1.0 to perform better trough preliminary testing. A thorough explanation of all the parameters, and their typical ranges can be found in the communication at the HyperNEAT tech group[1], as well as an argument posed by Gauci[2] on the difficulties in finding the "magic numbers" in terms of parameters when the complexity of a problem is of a considerable scale. This is intuitive because

[1] http://tech.groups.yahoo.com/group/neat/message/5299
[2] http://tech.groups.yahoo.com/group/neat/message/4498

when the complexity of the problem results in relatively long execution times per run, then the task of finding a "magic number" for any given parameter, for a total of 33 parameters and all of their permutations, is at least as time consuming as running the problem itself. Since our problem is of considerable complexity, where single runs easily could last for around 20 minutes, we had to restrict our preliminary testing of parameters to a qualitative analysis of the performance of a few runs with parameter values within the typical ranges that converged to relatively stable solutions.

Each run involved 100 individuals (CPPNs that encodes for a substrate) which were allowed to evolve for 100 generations. The fitness of each individual, for each of the 100 generations, was determined by the distance between the vectors outputted by the substrate and the target vectors. Equation 4.1 is the formal definition of our fitness function.

$$fitness(I) = \frac{1}{1 + \sum_{i=1}^{2} \sqrt{\sum_{j=0}^{n} |u_{ij} - v_{ij}|^2}} \tag{4.1}$$

The problem of detecting and correctly outputting the two dimensional value of the two emotions per subject was performed 20 times for each subject included, in order to get a bigger picture of the actual performance and robustness of our model. From the 200 runs performed, an average fitness of 0.806 ± 0.117 is achieved. This is calculated by taking the average of the winning solutions from each of the 20 runs for each of the subjects, with all their different pairs of affective ratings. Figure 4.3 shows the result of this quantitative approach as a fitness progression per generation, where the blue lines is the average of the 20 runs from one subject, accompanied by the standard deviation from each of these 20 runs (green lines). The red line is the overall average, as explained above, with the magenta line representing the standard deviation for the overall average. We chose include all the single subject runs and their standard deviation in the graph, in order to make a graphical representation of the variation in the results.

Three distinct run types can be seen from the single subject curves (blue) in figure 4.3. The first is the type where evolution quickly finds a good solution, typically within the first 10-20 generations, and ends up with a high winning fitness (> 0.95). The second is the type where the first 30+ generations is below the mean curve (red), and has an overall more linear growth from the starting fitness until approximately 0.8 where it gradually stabilizes. The third type is represented by the curves that are situated around the overall mean, and has a strong resemblance to the progression of the overall mean.

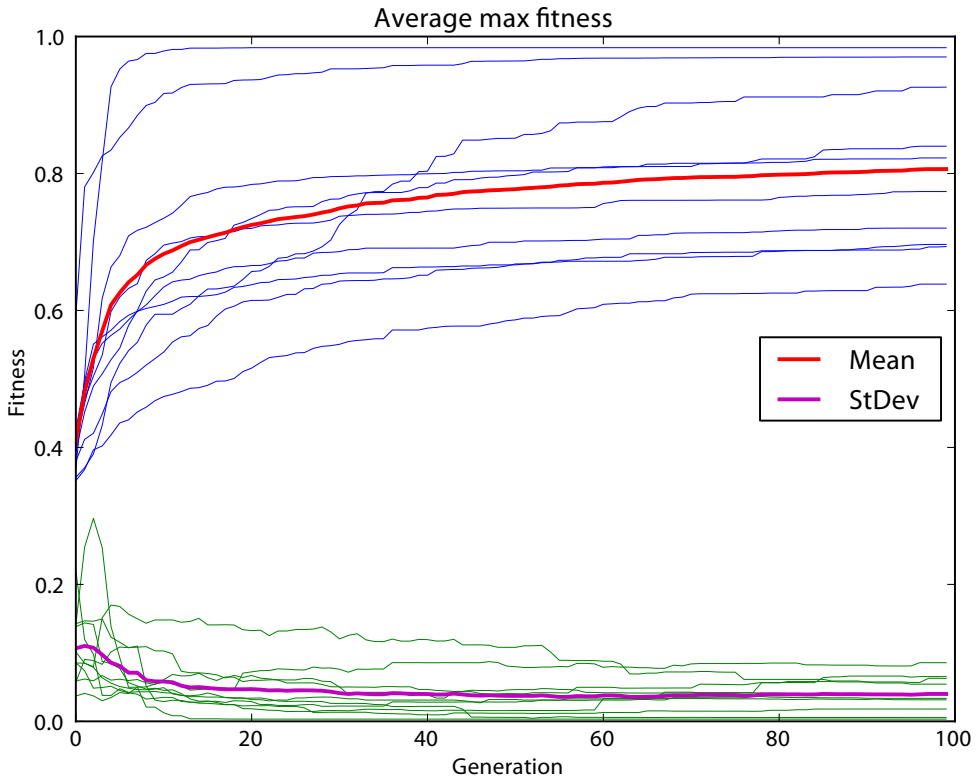

Figure 4.3: The fitness progression from all the runs. Blue curves are the mean of the best fitness for each of the 20 runs for one subject, accompanied by the standard deviation (green). The red curve is the overall mean fitness progression for all of the included subjects and runs, accomapnied by its standard deviation (magenta)

A difference in the initial fitness, and the initial rate of growth in fitness, from single runs in evolutionary systems is normally due to the randomized initial setup; some individuals gets a lucky start while others do not. However, the difference in the rate of growth in fitness in the three types mentioned above can probably not be explained by this phenomenon since the progression is an average of a substantial amount of runs, pointing towards a tendency that this average is in fact a good representation for the progression of a run with that distinct subject and trail combination. It is thus a representation of the difficulties in correctly detecting the patterns presented, in terms of the geometry, projected as a fitness value through the HyperNEAT methodology.

Table 4.2 shows how the results from each subject contribute to the total estimated fitness, where the first column is the subject number followed by the maximum and minimum fitness for the 20 runs performed on that subject's max/min pair of rating and EEG data. We can see here that even if the range restricted by the

maximum and minimum, in terms of the fitness from each of the 20 runs (which denotes the best and worst performing solutions), is relatively large, the inter-subject standard deviation is relatively low with a 0.04 ± 0.026 mean. This highlights two important aspects, where the first is that there is a tendency that solutions evolved for the same subject and same EEG-data are located near the mean for that particular setup. This gives confidence in the overall stability of this training method and setup; one can expect similar performance given similar data. The second is that the stability mentioned above is limited by qualitatively looking at the min/max ranges, which shows that there is no guarantee for a lowest performing solution with evolutionary function approximation within a finite time window (which of course any practical and useable system is restricted by)

Table 4.2: Performance per subject

Sub. num.	Max fit.	Min fit.	Mean fit.	St. dev.
01	0.883	0.725	0.774	0.031
02	0.996	0.980	0.984	0.003
03	0.804	0.502	0.638	0.086
04	0.983	0.963	0.970	0.006
05	0.986	0.728	0.926	0.054
06	0.974	0.770	0.840	0.065
07	0.856	0.800	0.823	0.018
08	0.869	0.634	0.693	0.063
09	0.732	0.592	0.696	0.040
10	0.800	0.648	0.720	0.034
Mean:	0.888	0.734	0.806	0.040
St. dev.:	0.088	0.145	0.117	0.026

Figure 4.4 shows our further investigation of the errors of the system. This is plotted in a similar fashion as figure 4.1, where the large dots is the target values given by the subject's ratings. The different colors of the large dots indicate different subjects and matching colors indicate the pairwise max/min ratings. The small dots are the actual ratings as outputted by the trained substrates, and a line is drawn from the outputs to the targets to illustrate their membership and to easily show the distance between the desired output and the actual output. Going back to figure 4.1 we noted that there was an interesting case where the maximum rating of subject 3 actually has negative valence (-0.0693), whereas the others cluster nicely between 0.5 and 1 in both the valence and arousal scale. A closer look at table 4.2 reveals that subject 3 also have the lowest mean fitness (0.638), and the highest standard

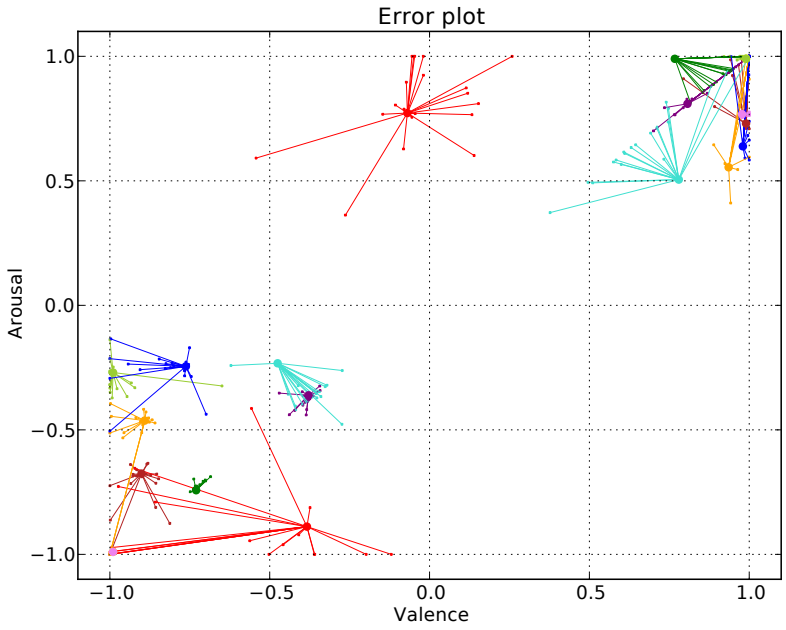

Figure 4.4: A graphical representation of all the errors produced by the evolved winning networks for all runs on all subjects. The color indicates a subject, where the big dots are the target ratings, and the small dots are the errors. Lines are drawn between the errors and their target values in order to easily identify their memebership as well as emphesize their distance from the target. It also enables us to look at the density of connections in different direction in order to detect distinct patterns (if any) in the errors produced

deviation (0.086) over the 20 runs.

The effect of this low mean fitness becomes pretty dramatic in figure 4.4. Subject 3, which is the identified by clear red colored dots at locations [-0.069, 0.772] and [-0.384, -0.889], has clearly the most widespread error network on both extremes in terms of rating. The density in connections from target to the error dots seem to be fairly denser in positive valence and arousal scale for the first point, and in negative valence scale for the second point. Subject 9 (turquoise) on the other hand, has the biggest density in a positive direction from the target in the valence scale, and in a negative direction in the arousal scale for the minimum rating. Subject 7 (dark green) has very little error overall for the minimum rating, and a density in connections towards positive valence and negative arousal, relative to the target. These three subjects have among the most widespread errors, and all of these have partly contradictory over/underestimations for both affective dimensions so there seem to be no obvious global error pattern directional wise with regards to these two dimensions.

A tendency to a pattern can be found in the positive quadrant for both dimen-

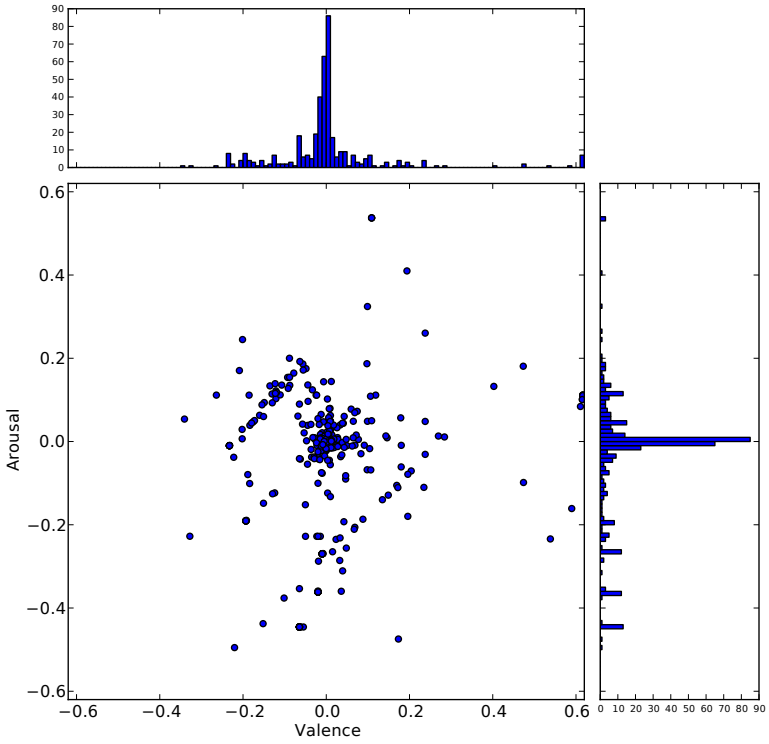

Figure 4.5: The distribution of all the 400 outputs produced by the 200 runs, where the offset from the middle is the relative distance from the target values to the output values produced by the winning individuals

sions, where the substrates evolved for dark green and turquoise seems to have a problem with separating the two outputs, and ends up with a similar value for both arousal and valence. This problem is apparent for turquoise in the negative quadrant as well, in a symmetrical but opposite direction and might suggest a problem with rotation because of overgeneralization with this subject. The dark green's target in the negative quadrant has near identical values in both directions, and is approximated quite well. One may be lead to the conclusion that it is symmetry that forces the dark green's approximations to the maximum rating to end up with near identical outputs for both dimensions, which may be the case. However, a quick look at light green (subject 5) reveals that even if the maximum rating has equal values in both dimensions [0.99, 0.99], the minimum value is approximated quite good even though being asymmetrical, which is contradictory to the assumptions of that symmetry on one of the ratings (maximum of minimum) results in symmetry of a potential asymmetric opposite rating. The relative distance from the asymmetric part of dark green is then again closer to being symmetric, so a definite conclusion is hard to obtain.

Figure 4.5 shows the relative distribution of errors from all the 400 outputs

produced by the 200 winning solutions in the two dimensions, where every blue dot is a single output (from either a maximum or a minimum rating), and the width of the histogram bins is 0.01 in actual distance in the dimension measured. This is an interesting plot because it allows us to investigate if the model has any biases or weaknesses in any directions in the two dimensions of emotion.

It is quite clear from figure 4.5 that most of the errors occurs within a ± 0.03 range, with a clear peak within ± 0.01, and thus speaks in favour of the accuracy of the model. An outer ring-like distribution can also be seen around the main cluster with a lowest accuracy of about ± 0.20, and makes up for most of the remaining error. The rest of the errors seem to be scattered in a randomly fashion, with only a couple of minor cluster in the negative part of the arousal dimension.

4.2 A Qualitative Explanation

The quantitative analysis shows a decent overall performance of the model with some minor errors evenly distributed in both dimensions, but was unable to explain or describe the standard deviation in performance per subject. We feel thus it is appropriate to investigate one of the individuals as an effort to uncover if there is any underlying explanation to the variations in the results.

From the previous section, we found that the substrates evolved for subject 3 resulted in a poor overall result and the highest intra-subject standard deviation (0.638 ± 0.086) for the 20 runs performed with the data from this subject. Subject 3 is therefore an interesting candidate to investigate. From the list of 20 runs from subject 3, the winning individual from run 8 with a fitness of 0.658 is chosen due to being closest to the overall mean fitness from all the 20 runs, and is hence close to an average performer for subject 3.

Figure 4.6 shows the winning CPPN from subject 3 run 8. It consists of 8 hidden nodes and 38 connections. There is a distinct difference between the two output nodes and how they are connected to the input nodes. The output node that paints the connective pattern between the input layer and output layer (right) is directly coupled to many of the input nodes, while the output node that paints the connective pattern between the hidden layer and the output layer (left) have considerably less such direct connections. This implicates that the function approximated for each of the two connective patterns have quite different complexity which naturally leads to patterns with quite different topologies.

The patterns painted by the CPPN are quite interesting by themselves, but they

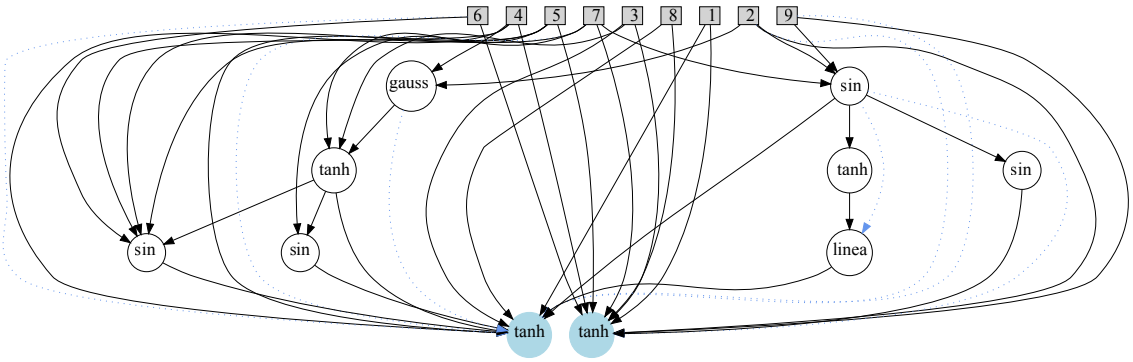

Figure 4.6: The pheontype (CPPN) from the winning individual, where squares represent the input nodes. The number of the input nodes are as follows: $[1, 2, 3, 4] = [x_1, y_1, R_1, H_1]$, $[4, 5, 6, 7, 8] = [x_2, y_2, R_2, H_2]$, and $9 = distance(endpoint_1, endpoint_2)$. The blue circles are the output nodes, where the left paints the connective pattern between the hidden layer and the output layer, and the right paints the connective pattern between the input layer and the hidden layer. The solid lines are active connections, and the dotted blue lines are disabled connections (as a result of mutation)

become more *meaningful* by first looking at the two trails from subject 3. Figure 4.8(a)–4.8(d) displays the activation topology for the two bands for each of the two trails, where (a) and (b) is the activation topology for the maximum rated trail, and (c) and (d) is for the minimum rated trail. Note that the activation maps are transformed back to the original 10-20 system in order to get standardized scalp plots. At first glance it is apparent that we are dealing with very similar, but not identical, activation patterns. There are clear peaks at Fc5 and P7 on the left hemisphere, and at Fc6 on the right hemisphere, for both trails and both bands. The peaks at Fc5 and P7 are slightly more intense at trail 33 than at trail 24, and the Fc6 at trail 24 beta activities is more intense than those from trail 33 beta activities. Moreover, the internal differences in Fc6 are clearer in trail 24 than what is seen in trail 33. The two cases are therefore separable, but only by small margins (< 0.1).

Figure 4.8(e)–4.8(h) shows the connective patterns produced by the CPPN in 4.6, where (e) shows the pattern as seen from the beta band (halo) in the hidden layer and (f) shows the pattern as seen from the gamma band (halo) in hidden layer. The two figures (g) and (h) show how the pattern between the hidden layer and output layer is seen from output node 1 (valence) and output node 2 (arousal) respectively.

From (e) and (f) we can see that the connective pattern between the input layer and hidden layer put an emphasis on the differences between the left and right

hemispheres, where (e) shows that the beta band has the least negative influence on the right hemisphere, and (f) shows that the gamma band has a positive influence on the right hemisphere and negative on the left hemisphere. Moving to (g) and (h) shows that the connective pattern between the hidden layer and the output layer is clearly more intricate, as predicted from the previous investigation of the CPPN. Furthermore, the difference in how the connective pattern is seen as receptive fields for the two output nodes, compared to how it is seen as receptive fields for the hidden layer, reveals that the connective pattern between the input layer and the hidden layer is following a global pattern between the two layers, and that the connective pattern between the hidden layer and the output layer is more specialized for each of the outputs.

The strategy of the substrate was easy to identify when looking at the receptive fields between the two first layers; it was a weighted difference between the left and right hemispheres. The strategy, as seen from the two output nodes are however harder to identify. If we look at figure 4.8(g) (valence), we can see that there is a strong positive influence from the Fc6 channel and an even stronger positive influence from the front/left channels (Af3, Af4, F3, F7, Fc5), as projected trough the hidden layer. The negative influence is located from T7 trough O2, in counter clockwise direction. This is an interesting observation, because if we look back at figure 4.8(a)–4.8(a), which show the difference in the two trails presented, we can see that the strongest positive influence is actually situated at a low activity area, where Fc5 is the only peak area (partly) included. Even though some differences between the two cases are apparent in this region, it is quite clear that this poses some problems with precision because of the similarity they exhibit.

Figure 4.8(h) shows a much simpler strategy for output node 2 (arousal), where it has the main positive influence from the Fc5 channel which we identified as easily differentiable from the two trails based on the visual inspection of the activation maps. One should then expect a better performance in the arousal dimension, but it turns out that both has a near identical relative error in both direction in total for both cases (approximately 0.3). The strategies combined are clearly not giving the desired performance in terms of precision of the outputs. One could of course be ignorant and blame it all on evolution by stating that evolutionary approximations come with no guarantee of finding a (near) optimal solution to the problem posed, but that would be akin to stating that evolutionary systems in general, and in this case neuroevolution, are poor problem-solvers. This is not the case, as we also have seen in the quantitative analysis, where the overall mean performance is good, along with excellent individual performance from the solutions found for specific subjects.

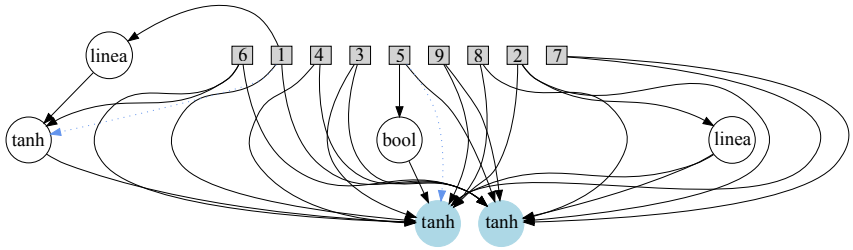

Figure 4.7: The phenotype (CPPN) from the winning individual of the 7th run from the 20 runs performed on the data from subject 2. The organization and layout is the same as seen in figure 4.6.

Let us then introduce subject 2, which is the test's best performer with an overall mean performance of 0.984, in an attempt to uncover why the variations in results from different subjects occur. From the 20 runs on the data from subject 2, we chose run 7 where the winning individual had a fitness of 0.985 and was thus close to an average performer.

Figure 4.7 shows the winning individual (CPPN) from subject 2 run 7. It is already evident when comparing with the CPPN from subject 3 run 8 (figure 4.6), in terms of complexity of the CPPNs, that we are dealing with less complex connective patterns. In fact, the CPPN from subject 2 got 4 hidden nodes and 26 connections, while the CPPN from subject 3 got 8 hidden nodes and 38 connections as previously mentioned, which shows two networks with totally different scales of complexity.

Before looking at the difference in the connective patterns produced, we also here find it beneficial to first have a look at the appearance of the training cases (min/max) from subject 2. Figure 4.9(a)–4.9(d) shows the activation plots of the training cases in the 10-20 system, similar to those previously seen for subject 3. If we define the peak areas of the plots as regions of interest, then there are 4 regions of interest seen in (a)–(d), located at F4, Af3, T7 and O2. These are present in both cases and in both bands. The T7 position has a high activation in trail 2 (max case) beta activities, accompanied by less activity at Af3 and F4, and a low peak at O2. The gamma activities in trail 2 are most present at Af3 and F4, and smaller peaks at T7 and O2. Trail 20 (min case) has high activity in F4, Af3, and T7, with a minor peak at O2 in the beta band. The gamma activities in trail 20 are primarily located at F4 and Af3, accompanied by smaller peaks in T7 and O2. This means that the inter-case dynamics is primarily located at F4 and Af3 in beta band activity, much like the one seen at the Fc5 location in subject 3.

The complexity of the activation patterns, in terms of numbers of regions of interest, is higher for subject 2 (4 peaks) than for subject 3 (3 peaks), which makes

the fact that the runs from subject 2 ended up with a much higher fitness than the runs from subject 3 even more interesting.

Figure 4.9(e)–4.9(h)shows the connective patterns produced between the layers of the substrate as receptive fields, from the different parts of the substrate which is identical in layout to those earlier seen for subject 3. From the hidden layer receptive fields, shown in (e) and (f), we can see that there is a main positive influence from the left hemisphere in the back area (T7, P7 and O1) in both hidden layer receptive fields. The negative influence extends from Af3 trough Fc5 for the hidden layer beta receptive field, and from Fc6 trough O2 for the hidden layer gamma receptive field. Even though there are differences in the negative influence area, the overall strategy from the connective pattern between the input layer and the hidden layer is clear, with a distinct line between the left back area and the front right area.

If we look at figure 4.9(g) and 4.9(h), we can also easily identify the overall strategy from the connective pattern between the hidden layer and the output layer. From the receptive fields for both output nodes we can see that there is a strong positive influence from the front right area (Af3 trough Fc5), with a negative influence in the left back area (Fc6 trough O2) for valence. This area is extended to include O2 for the second output node (arousal). The strategy does also easily counter low activity areas from the training cases, by giving them near zero influence which appears as green in (g) and (h).

The strategies evolved for subject 2 compared to subject 3 are much more general, and appear as smooth topologies in the receptive fields. Interestingly, the most general patterns evolved the most general (and best) players in the checkers experiment in (Gauci and Stanley, 2010), which also seems to be the case for the CPPNs evolved for detecting emotions in EEG signals. The general patterns produced for subject 2 do effectively use the regions of interest in their strategies (as weighted influence) and at the same time avoids low activity areas by giving them low influence. The less general patterns, as evolved from the data of subject 3, do not manage to use the regions of interest as effectively, and does in fact rely on low activity areas as part of their overall strategy instead of avoiding them, which results in lower mean performance with higher variations.

Another interesting finding is that the complexity of the training cases seems to be of little significance to the strategies evolved; the more complex training cases from subject 2 resulted in a more general solution and an overall higher mean performance than the solutions found for the less complex training cases from subject 3. One main difference between the cases from the different subjects is the relative

difference in power from the peak regions between the intra-subject minimum and maximum case, where the difference is biggest in the cases from subject 2. This suggests that precision is a potential problem when evolving substrates with HyperNEAT, and that this is causing the evolved solutions to be less general and lower performing than solutions evolved for substrates where the problem of finding a good solution requires less precision.

The explanation for this problem might be intricate, but a look back at how NEAT evolves networks might give an indication of where to start. NEAT explores the search space for a solution from a minimal structure, and gradually increases this space by adding new nodes and connection to individuals through mutations. If the current search space is not investigated thoroughly, when high precision is required (low relative distance between a poor and an excellent performance), then mutations that only slightly increase the fitness of an individual stands out as the current best solution. This will gradually lead to the disappearance of the genes from individuals in the populations that are close to the most general and/or near optimal solution, but are unable to find it unless a lucky mutation occurs. We can find traces of this in the runs performed on the data from subject 3, where the best run resulted in a fitness of 0.804 and the worst run resulted in a fitness of 0.502, with a mean overall fitness of 0.638.

This problem is essentially quite similar to having a too high learning rate in supervised learning algorithms like backpropagation, where any adjustment to the weight is causing the algorithm to miss the lowest point on the error curve. One solution to this problem in NEAT could then be to lower the weight mutation power (how much a weight are allowed to change in one mutation), but this could again lead to very slow convergence and the potential for that adding new nodes and connections would still be the most effective way to slightly (but inappropriately) increase the fitness, which again could lead to the loss of the genes that are close to a general and good solution and takes us back to square one. Another problem with fine-tuning the weight mutation power is finding the correct mutation rate for all the cases posed, which will be more time consuming than the actual solving of the problem, as mentioned earlier. An adaptive change in the mutation power seems to be more appropriate. This could be realized by the same principles as the adjustments of the momentum term often used in backpropagation, and thereby allow the mutation power to be high or low depending on the previous relative gains.

Another approach to this problem is to modify NEAT to allow for learning algorithms in the postnatal state, before the fitness assessment. The changes made through learning could easily be stored, since NEAT after all uses direct encoding.

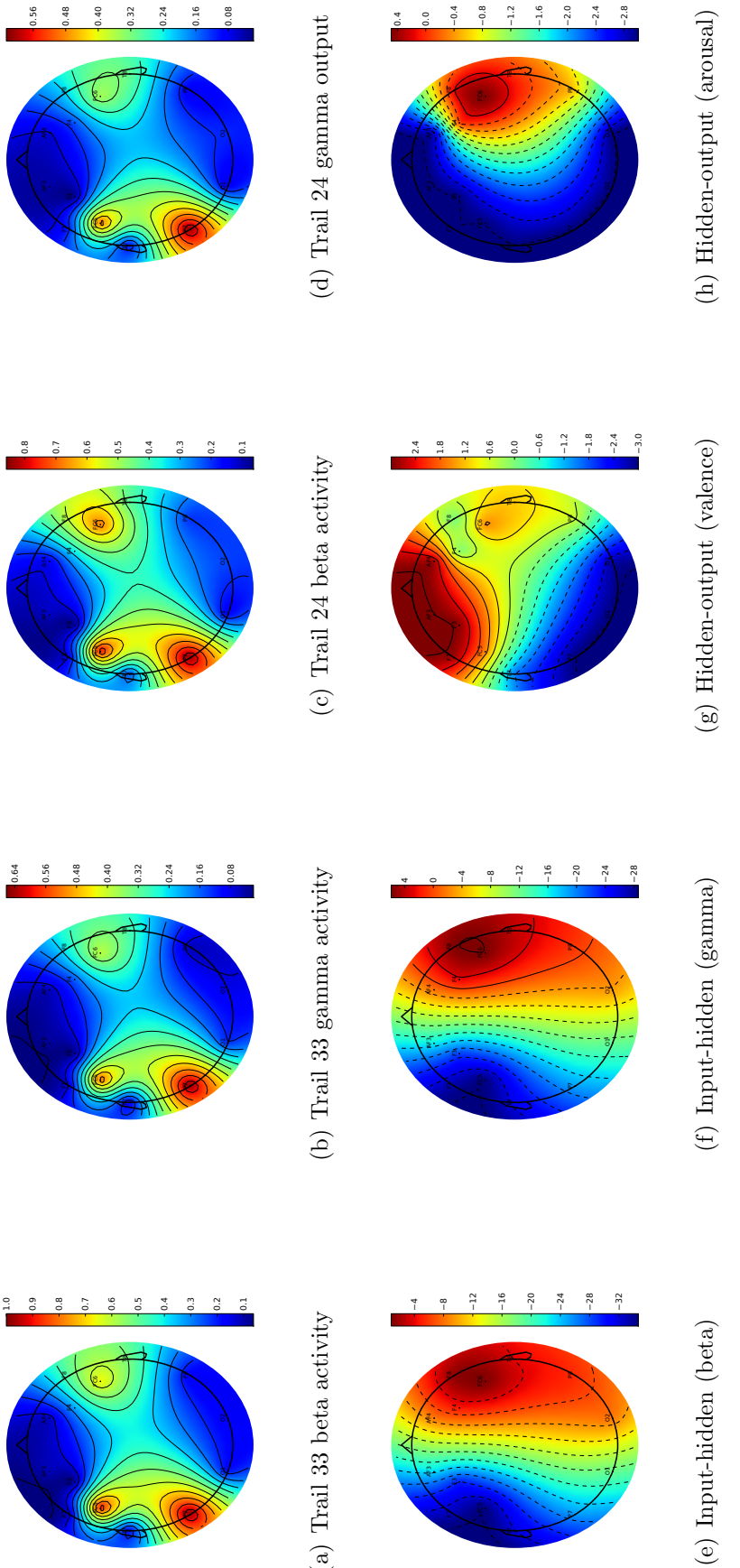

(a) Trail 33 beta activity (b) Trail 33 gamma activity (c) Trail 24 beta activity (d) Trail 24 gamma output

(e) Input-hidden (beta) (f) Input-hidden (gamma) (g) Hidden-output (valence) (h) Hidden-output (arousal)

Figure 4.8: This figure is essentially split in two different parts, but these two parts are most valuable when seen together. Figure 4.8(a)–4.8(d) shows the two different trails (pre-processed according Chapter 3) from subject 3 as activation plots in the 10-20 system. Figure 4.8(e)–4.8(h) shows the connective patterns produced by the winning CPPN from run 8 with the trails from subject 3, as seen from different parts of the substrate (receptive fields from the parts indicated by the text under the figures), plotted in the 10-20 system.

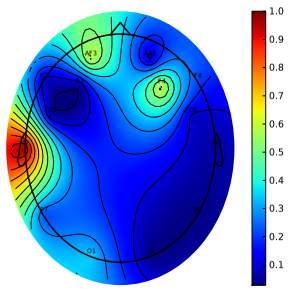

(a) Trail 2 beta activity

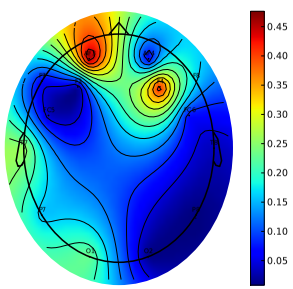

(b) Trail 2 gamma activity

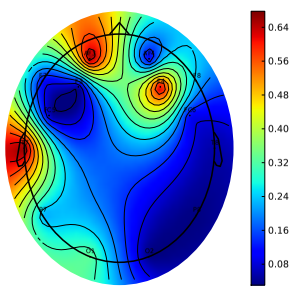

(c) Trail 20 beta activity

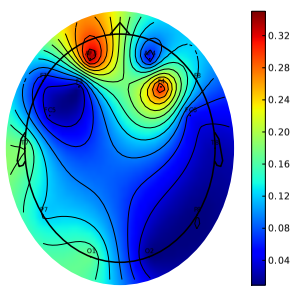

(d) Trail 20 gamma output

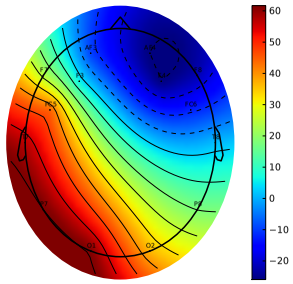

(e) Input-hidden (beta)

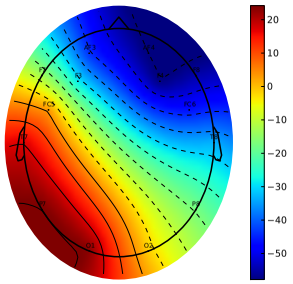

(f) Input-hidden (gamma)

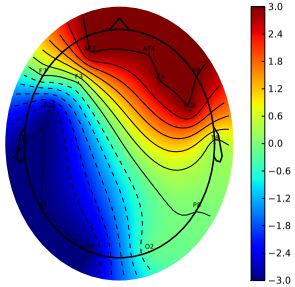

(g) Hidden-output (valence)

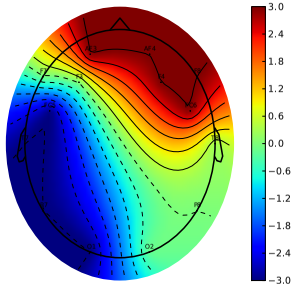

(h) Hidden-output (arousal)

Figure 4.9: 4.9(a)–4.9(d) shows the two different trails from subject 2, as activation plots in the 10-20 system. Figure 4.8(e)–4.8(h) shows the connective patterns produced by the winning CPPN from run 7 with the trails from subject 2, as seen from different parts of the substrate (receptive fields from the parts indicated by the text under the figures), plotted in the 10-20 system.

Chapter 5

Conclusion & Future Work

We have in this thesis conducted a thorough investigation of the problem areas in order to propose a model for detecting emotions by the use of ANN. This resulted in a better understanding of what emotions are, and how such a subjective phenomenon can be measured and described in terms of a recognized universal model. The dependent two-dimensional model of emotions allowed us to generalize over the cognitive structure of interpretations of emotions, instead of a subjective description. We have by that avoided a generalization over pure subjectivity, and thus reduced the uncertainty about the results we have seen when testing. This reduction in uncertainty is however limited by the validity of the two-dimensional model as a universal model of emotion.

The investigation of EEG resulted in an overview of the common computational methods used for analysis of the signal, and what to expect as result when transforming a signal that is non-stationary, non-linear, and noisy by nature. Further, the analysis of the actual EEG signal allowed us to identify frequency ranges with minimized variance, and hence the identification of the most appropriate frequency ranges to generalize over in terms of the accuracy of the power estimates of the underlying stochastic processes.

Our exploration of BCIs provided a foundation for the most common techniques used to enable humans to communicate with machines, in a meaningful manner, through brain activity. The model we created for detecting of emotions through EEG can easily be placed in the first category from the three categories of BCIs listed in Chapter 2.3. The first category is where the system adapts to the user completely, so our model does therefore avoid the ethical question we raised concerning self-inflicted neuroplasticity from uncontrolled use, because there is no training or adaptation needed from a user in order to achieve full functionality from the system.

The related BCI systems we found do mostly rely on features extracted from the signal. This entails a subjectivity involved when choosing methods to extract the features, and that an ANN trained on these features approximates a function of these features instead of the problem itself. Our model minimizes this subjectivity by expressing the signal by its mean power as a function of frequencies, linearly transformed by FFT, and presenting it to the ANN in an adapted version of the basic geometry of the problem. The only assumptions made here, is that the signal is better described when transformed into the frequency domain, and that the mean of N transformed time frames of the signal is a better estimate of the underlying rhythms encoding for an emotional state, than what each of the single time frames or the total trail is. The nature of the signal, and therefore also the problem, is hence preserved.

This highlights an important aspect of this thesis; the preservation of geometrical information in the multi-channel signal, through pre-processing instead of extensive feature extraction, allow us to use a method for detection of emotions that evolves ANNs on the basis of the basic geometry of the problem, which is more in line with the true nature of the problem. Seen the other way around, reveals that by identifying EEG as a geometrical problem (oscillating signal recorded from different positions on the skull), and using a method (HyperNEAT) that is proven to perform well on geometrical problems, allowed us to reduce the computational overhead of feature extraction to lightweight pre-processing, as well as avoiding the subjectivity involved with choosing what features to extract.

An interesting bi-product of this approach is that because the ANNs is evolved on the basis of the basic geometry of the problem, which entails that the nodes in the ANNs have distinct positions in space, the connective patterns as seen as receptive fields from any chosen part of the system can easily be interpreted into meaningful strategies. This allow for an investigation and understanding of the behaviour of ANNs that we not have seen this clearly with any other methods for evolving or training ANNs.

The experimental results in this thesis shows a promising high mean overall performance (0.806 in fitness), with some variations (0.116 standard deviation) introduced by the different performance from the individual 20 runs per subject. Our investigation of the errors produced, revealed that these variations was not caused by any problems with detecting any of the two-dimensions in both directions, and that only 6 of 400 outputs ended up in a wrong quadrant. Further, we found that most of the errors occur within a precision range of ± 0.01 in both dimensions. A possible explanation for the standard deviation in the overall performance was found during

our qualitative analysis of the individuals produced for the best and worst overall performance per subject. This qualitative analysis of training cases and strategies evolved (seen as receptive fields from different parts of the ANNs), points in a direction where HyperNEAT struggles to evolve general strategies that use regions of interest (peak activation areas) when high precision is needed in order to correctly distinguish them from one another in the training cases. The underlying cause of this problem may stem from how CPPN-NEAT gradually evolves more complex patterns, and thereby a gradually bigger search space. If the search space that contains the most general and/or near optimal solution is not *correctly* investigated, then a gradual loss of genes from the individuals in that particular search space may occur if evolution finds slightly fitter individuals by adding nodes or connections.

We suggest that a possible solution to this NEAT-specific problem is to lower the weight mutation power, and allow for smaller movements in the search space. This may however result in a too slow convergence, and a possibility for that adding nodes and connections provides the fastest (but inappropriate) increase in fitness, which could lead to bloating and the loss of the same genes as with high weight mutation power. Also, building statistics around different values of weight mutation power (and possibly other parameters) for a given problem in order to determine a *magic number*, is at least as time consuming as solving the problem itself, and thus becomes less and less attractive as the complexity of the problem increases. We hence consider our two other suggestions, adaptive change in weight mutation power (which could be extended to other parameters as well), and/or the inclusion of learning in the postnatal state of the CPPNs, as more interesting and probable solutions which we find worth pursuing on a general basis in the future.

Even though the experimental results are promising with regards to the capability of HyperNEAT as a method used in the area of detecting human emotions through EEG, it is clear that more testing is needed before we can conclude on its general viability in the problem area. We do also recognize that the standard deviation in the overall results is an indicator of some limitations of using HyperNEAT to evolve ANNs that require a relatively high degree of precision in order to correctly approximate the function needed to get the outputs in the precision desired, when only small margins separates the training cases, and is thus a limitation in our model. This limitation can possibly be addressed by the suggestions we made earlier regarding CPPN-NEAT, and is our first priority in the future work of tuning and stabilizing our model.

The results do also give strong indications that a commercially available EEG headset such as Emotiv EPOC with limited resolution in terms of electrodes, in

combination with our model, is indeed sufficient to detect emotions from humans. Adding the fact that our model, as a BCI, poses no ethical issues because it completely adapts to the user, means that our (or similar) model can both freely and safely be distributed to the public. This supports our vision and desires of integrating human emotions in the concept of rationality in machines that interact with humans, in an attempt to address the problems associated with *rationality mismatch*, which could lead to more intelligent interaction between man and machine.

Appendix A

Parameters

HyperNEAT parameters

```
[phenotype]
    input_nodes = 9
    output_nodes = 2
    fully_connected  = 1
    max_weight = 5
    min_weight = -5
    feedforward = 1
    hidden_nodes = 0
    weight_stdev = 2.9

[genetic]
    pop_size = 100
    max_fitness_threshold = 0.98
    elitism = 1
    tournament_size = 2
    tournament_p = 1.0
    prob_addconn = 0.05
    prob_addnode = 0.03
    prob_mutatebias = 0.26
    bias_mutation_power = 0.21
    prob_mutate_weight = 0.8
    weight_mutation_power = 1.0
    prob_togglelink = 0.05
```

```
[genotype compatibility]
    compatibility_threshold = 6.0
    compatibility_change = 0.3
    excess_coeficient = 2.0
    disjoint_coeficient = 2.0
    weight_coeficient = 1.0

[species]
    species_size = 6
    survival_threshold = 0.2
    old_threshold = 30
    youth_threshold = 10
    old_penalty = 0.2
    youth_boost = 1.2
    max_stagnation = 15
```

Bibliography

Berka, C., Levendowski, D. J., Cvetinovic, M. M., Petrovic, M. M., Davis, G., Lumicao, M. N., Zivkovic, V. T., Popovic, M. V., and Olmstead, R. (2004). Real-time analysis of eeg indexes of alertness, cognition, and memory acquired with a wireless eeg headset. *International Journal of Human-Computer Interaction*, 17(2):151–170.

Bradley, M. M. and Lang, P. J. (1994). Measuring emotion: the self-assessment manikin and the semantic differential. *Journal of behavior therapy and experimental psychiatry*, 25(1):49–59.

Conte, H. and Plutchik, R. (1981). A circumplex model for interpersonal personality traits. *Journal of Personality and Social Psychology*, 40(4):701.

Cooley, J. W. and Tukey, J. W. (1965). An algorithm for the machine calculation of complex fourier series. *Math. Comput*, 19(90):297–301.

Dan, S. and Robert, S. (2011). An exploration of the utilization of electroencephalography and neural nets to control robots. *An Exploration of the Utilization of Electroencephalography and Neural Nets to Control Robots*, 6949.

De Sousa, R. (2012). Emotion. *The Stanford Encyclopedia of Philosophy*.

Ekman, P. (1992). An argument for basic emotions. *Cognition & Emotion*, 6(3-4):169–200.

Ekman, P. (1999). *Basic Emotions*, chapter 3, pages 45–60. John Wiley & Sons, Ltd.

Ekman, P. and Friesen, W. V. (1971). Constants across cultures in the face and emotion. *Journal of Personality and Social Psychology*, 17(2):124–129.

Floreano, D., Dürr, P., and Mattiussi, C. (2008). Neuroevolution: from architectures to learning. *Evolutionary Intelligence*, 1(1):47–62.

Gauci, J. and Stanley, K. O. (2010). Autonomous evolution of topographic regularities in artificial neural networks. *Neural Computation*, 22(7):1860–1898.

Gauci, J. and Stanley, K. O. (2011). Indirect encoding of neural networks for scalable go. *Parallel Problem Solving from Nature–PPSN XI*, pages 354–363.

Gomez, F. J. and Miikkulainen, R. (1999). Solving non-markovian control tasks with neuroevolution. volume 16, pages 1356–1361. LAWRENCE ERLBAUM ASSOCIATES LTD.

Grierson, M. (2011). Better brain interfacing for the masses: progress in event-related potential detection using commercial brain computer interfaces. *CHI EA '11: Proceedings of the 2011 annual conference extended abstracts on Human factors in computing systems*.

Gruau, F., Whitley, D., and Pyeatt, L. (1996). A comparison between cellular encoding and direct encoding for genetic neural networks. pages 81–89. MIT Press.

Gwin, J. T., Gramann, K., Makeig, S., and Ferris, D. P. (2010). Removal of movement artifact from high-density eeg recorded during walking and running. *J Neurophysiol*, 103(6):3526–34.

Haralick, R., Shanmugam, K., and Dinstein, I. (1973). Textural features for image classification. *Systems, Man and Cybernetics, IEEE Transactions on*, 3(6):610–621.

Hjorth, B. (1970). Eeg analysis based on time domain properties. *Electroencephalography and clinical neurophysiology*, 29(3):306–310.

Horlings, R., Datcu, D., and Rothkrantz, L. J. M. (2008). Emotion recognition using brain activity. In *Proceedings of the 9th International Conference on Computer Systems and Technologies and Workshop for PhD Students in Computing*, pages II.1–1, 1500888. ACM.

Juan Manuel, R.-C., Vicente, A.-A., Gerardo, R.-C., Pilar, G.-G., and Jorge, E.-A. (2011). Anfis-based p300 rhythm detection using wavelet feature extraction on blind source separated eeg signals. *Anfis-Based P300 Rhythm Detection Using Wavelet Feature Extraction on Blind Source Separated Eeg Signals*, 103.

Khosrowabadi, R., Hiok Chai, Q., Wahab, A., and Kai Keng, A. (2010). Eeg-based emotion recognition using self-organizing map for boundary detection. In *Pattern Recognition (ICPR), 2010 20th International Conference on*, pages 4242–4245.

Kitano, H. (1990). Designing neural networks using genetic algorithms with graph generation system. *Complex Systems Journal*, 4:461–476.

Klonowski, W. (2007). From conformons to human brains: an informal overview of nonlinear dynamics and its applications in biomedicine. *Nonlinear Biomed Phys*, 1(1):5.

Klonowski, W. (2009). Everything you wanted to ask about eeg but were afraid to get the right answer. *Nonlinear Biomed Phys*, 3(1):2.

Koelstra, S., Muhl, C., Soleymani, M., Lee, J., Yazdani, A., Ebrahimi, T., Pun, T., Nijholt, A., and Patras, I. (2011). Deap: A database for emotion analysis using physiological signals. *Affective Computing, IEEE Transactions on*, (99):1–15.

Kvaale, S. P. (2011). Detection of mood through analysis of brainwaves. Technical report, Norwegian University of Science and Technology.

Leighton, S. R. (1982). Aristotle and the emotions. *Phronesis*, 27(2):144–174.

Levine, S. P., Huggins, J. E., BeMent, S. L., Kushwaha, R. K., Schuh, L. A., Passaro, E. A., Rohde, M. M., and Ross, D. A. (1999). Identification of electrocorticogram patterns as the basis for a direct brain interface. *J Clin Neurophysiol*, 16(5):439–47.

Malmivuo, J. and Plonsey, R. (1995). *Bioelectromagnetism: principles and applications of bioelectric and biomagnetic fields*, chapter 13, pages 257–264. Oxford University Press, USA.

Maybury, M. (1999). Intelligent user interfaces: an introduction. In *Proceedings of the 4th international conference on Intelligent user interfaces*, pages 3–4, 291081. ACM.

McFarland, D. J. and Wolpaw, J. R. (2011). Brain-computer interfaces for communication and control. *Commun. ACM*, 54(5):60–66.

Miller, G. F., Todd, P. M., and Hegde, S. U. (1989). Designing neural networks using genetic algorithms. In *Proceedings of the third international conference on Genetic algorithms*, pages 379–384, 94034. Morgan Kaufmann Publishers Inc.

Miner, L. A., McFarland, D. J., and Wolpaw, J. R. (1998). Answering questions with an electroencephalogram-based brain-computer interface. *Arch Phys Med Rehabil*, 79(9):1029–33.

Mohler, H., Fritschy, J. M., and Rudolph, U. (2002). A new benzodiazepine pharmacology. *J Pharmacol Exp Ther*, 300(1):2–8.

Montana, D. J. and Davis, L. (1989). Training feedforward neural networks using genetic algorithms. volume 1, pages 762–767. San Mateo, CA.

Mustafa, M., Taib, M. N., Murat, Z. H., Sulaiman, N., and Aris, S. A. M. (2011). The analysis of eeg spectrogram image for brainwave balancing application using ann. In *Computer Modelling and Simulation (UKSim), 2011 UkSim 13th International Conference on*, pages 64–68.

Nowlis, V. and Nowlis, H. H. (1956). The description and analysis of mood. *Annals of the New York Academy of Sciences*, 65(4):345–355.

Nunez, P. L. and Srinivasan, R. (2006). *Electric fields of the brain: the neurophysics of EEG*. Oxford University Press, USA.

Nunez, P. L. and Srinivasan, R. (2007). Electroencephalogram. *Scholarpedia*, 2:1348.

Petersen, M., Stahlhut, C., Stopczynski, A., Larsen, J., and Hansen, L. (2011). *Smartphones Get Emotional: Mind Reading Images and Reconstructing the Neural Sources Affective Computing and Intelligent Interaction*, volume 6975 of *Lecture Notes in Computer Science*, pages 578–587. Springer Berlin / Heidelberg.

Plutchik, R. (2000). *A psychoevolutionary theory of emotion*, chapter 4, pages 59–79. American Psychological Association, Washington, DC, US.

Plutchik, R. (2001). The nature of emotions: Human emotions have deep evolutionary roots, a fact that may explain their complexity and provide tools for clinical practice. *American Scientist*, 89(4):344–350.

Ros, T., Munneke, M. A. M., Ruge, D., Gruzelier, J. H., and Rothwell, J. C. (2010). Endogenous control of waking brain rhythms induces neuroplasticity in humans. *European Journal of Neuroscience*, 31(4):770–778.

Russell, J. A. (1980). A circumplex model of affect. *Journal of Personality and Social Psychology*, 39(6):1161–1178.

Sanei, S. and Chambers, J. A. (2008). *EEG Signal Processing*. Wiley, Hoboken, NJ, USA.

Schaeffer, J., Burch, N., Björnsson, Y., Kishimoto, A., Müller, M., Lake, R., Lu, P., and Sutphen, S. (2007). Checkers is solved. *Science*, 317(5844):1518–1522.

Schlosberg, H. (1952). The description of facial expressions in terms of two dimensions. *Journal of Experimental Psychology; Journal of Experimental Psychology*, 44(4):229.

Schlosberg, H. (1954). Three dimensions of emotion. *Psychological review*, 61(2):81.

Sharbrough, F., Chatrian, G. E., Lesser, R. P., Luders, H., Nuwer, M., and Picton, T. W. (1991). American electroencephalographic society guidelines for standard electrode position nomenclature. *Clinical Neurophysiology*, (8):200–202.

Solomon, R. C. (2010). *The philosophy of emotions*, chapter 1, pages 3–15. Guilford Press, 3 edition.

Sourina, O. and Liu, Y. (2011). A fractal-based algorithm of emotion recognition from eeg using arousal-valence model. In *Biosignals 2011*, pages 209–214. Springer.

Stanley, K. O. (2006). Exploiting regularity without development. In *AAAI Fall Symposium on Developmental Systems*. AAAI Press.

Stanley, K. O. (2007). Compositional pattern producing networks: A novel abstraction of development. *Genetic Programming and Evolvable Machines*, 8(2):131–162.

Stanley, K. O., D'Ambrosio, D. B., and Gauci, J. (2009). A hypercube-based encoding for evolving large-scale neural networks. *Artif. Life*, 15(2):185–212.

Stanley, K. O. and Miikkulainen, R. (2002a). Efficient evolution of neural network topologies. volume 2, pages 1757–1762. IEEE.

Stanley, K. O. and Miikkulainen, R. (2002b). Evolving neural networks through augmenting topologies. *Evolutionary computation*, 10(2):99–127.

Stern, J. M. and Engel, J. (2005). *Atlas of EEG patterns*. Lippincott Williams & Wilkins, Philadelphia.

Toga, A. and Thompson, P. (2003). Mapping brain asymmetry. *Nature Reviews Neuroscience*, 4(1):37–48.

Van Erp, J., Lotte, F., and Tangermann, M. (2012). Brain-computer interfaces: Beyond medical applications. *Computer*, 45(4):26–34.

Van Lier, H., Drinkenburg, W. H. I. M., van Eeten, Y. J. W., and Coenen, A. M. L. (2004). Effects of diazepam and zolpidem on eeg beta frequencies are behavior-specific in rats. *Neuropharmacology*, 47(2):163–174.

Welch, P. (1967). The use of fast fourier transform for the estimation of power spectra: a method based on time averaging over short, modified periodograms. *Audio and Electroacoustics, IEEE Transactions on*, 15(2):70–73.

Wolpaw, J. R., Birbaumer, N., McFarland, D. J., Pfurtscheller, G., and Vaughan, T. M. (2002). Brain-computer interfaces for communication and control. *Clin Neurophysiol*, 113(6):767–91.

Wolpaw, J. R., McFarland, D. J., Neat, G. W., and Forneris, C. A. (1991). An eeg-based brain-computer interface for cursor control. *Electroencephalography and clinical neurophysiology*, 78(3):252–259.

Wolpaw, J. R., Ramoser, H., McFarland, D. J., and Pfurtscheller, G. (1998). Eeg-based communication: improved accuracy by response verification. *Rehabilitation Engineering, IEEE Transactions on*, 6(3):326–333.

Woolley, B. and Stanley, K. O. (2011). Evolving a single scalable controller for an octopus arm with a variable number of segments. *Parallel Problem Solving from Nature–PPSN XI*, pages 270–279.